Structural and Kinetic studies of Acyl-CoA Carboxylases in Mycobacterium tuberculosis

GEORGE CHAPPELL

Structural and Kinetic studies of Acyl-CoA Carboxylases in *Mycobacterium tuberculosis*

Master thesis

submitted to the

Department of Biosciences at Durham University, United Kingdom

for the degree of

Master of Research in Biological Sciences

George Thomas Chappell

2020

Table of Contents

Abbreviations

ACC	Acetyl-coenzyme A carboxylase
ACP	Acyl carrier protein
ADP	Adenosine diphosphate
AG	Arabinogalactan
ATP	Adenosine triphosphate
BC	Biotin carboxylase
BCCP	Biotin carboxyl carrier protein
β-ME	Beta-mercaptoethanol
BSA	Bovine serum albumin
CoA	Coenzyme A
CT	Carboxyltransferase
Da	Dalton
ddH_2O	Double distilled water
DESY	Deutsches Elektronen Synchrotron
EM	Electron microscopy
FAS	Fatty acid synthase
GA	Glutaraldehyde
GC	Guanine-Cytosine
HEPES	4-(2-hydroxyethyl)-1-piperazineethanesulfonic acid
His	Histidine
HIV	Human immunodeficiency virus
Hyg	Hygromycin
IMAC	Immobilized metal affinity chromatography
INH	Isoniazid
IPTG	Isopropyl β-D-1-thiogalactopyranoside
Kan	Kanamycin
kDa	Kilodalton
LB	Luria broth
mAU	Milli-absorbance unit
MCS	Multiple cloning site
MDR-TB	Multidrug-resistant tuberculosis
MW	Molecular weight
Mtb	Mycobacterium tuberculosis
NADH	Nicotinamide adenine dinucleotide (reduced)
NEB	New England Biolabs
NTA	Nitrilotriacetic acid
OD_{600}	Optical density at 600 nm
ORF	Open reading frame
PAGE	Polyacrylamide gel electrophoresis
PG	Peptidoglycan
PKS	Polyketide synthase
PZA	Pyrazinamide
RE	Restriction Enzyme
RIF	Rifampicin

ROS	Reactive oxygen species
SDS	Sodium dodecyl sulphate
SEC	Size exclusion chromatography
SEM	Scanning electron microscopy
SOC	Super optimal catabolite repression medium
SLiCE	Seamless Ligation Cloning Extract
SUMO	Small ubiquitin-like modifier
TB	Terrific broth
TB	Tuberculosis
TCEP	Tris-(2-carboxyethyl)-phosphine
TEM	Transmission electron microscopy
TEV	Tobacco Etch Virus
TRNA	Transfer RNA
T7SS	Type VII secretion system
UN	United Nations
UV	Ultraviolet
(v/v)	Volume/volume
WHO	World Health Organisation
(w/v)	Weight/volume
XDR-TB	Extremely drug-resistant tuberculosis
YCC	Acyl-CoA carboxylase

Abstract

Mycobacterium tuberculosis is a pathogen responsible for around 10 million new TB cases and 1.4 million deaths per year, making it the primary cause of death from an infectious agent. A range of effective treatments are available, typically involving complex and lengthy protocols. Difficulties in treatment can arise with incorrect prescription and adherence to these protocols alongside the emergence of drug-resistant TB. This has generated a pressing need for improved TB therapies. The cell wall of *M. tuberculosis* is a complex structure with a diverse array of unique molecules such as mycolic acids. This complexity of lipids can provide *M. tuberculosis* with increased virulence capacity, but also resistance to antibiotics. Lipid metabolism pathways used to synthesise the unique mycolic acid components have become attractive therapeutic targets, with acyl-CoA carboxylase (YCC) enzymes functioning at the committed step of their biosynthesis. YCC enzymes are composed of biotin carboxylase-biotin carboxyl carrier protein (α) and carboxyltransferase (β) subunits. So far, whole complex structures are yet to be determined. This information could be essential to future drug design. This study is focussed on structural and kinetic characterisation of subunits relevant to mycolic acid synthesis, some of which include AccA3 (α), AccD5 (β) and AccE5 (ε) together forming an enzyme complex, the latter subunit proposed to improve complex stability. Co-expression and co-purification strategies were used to isolate our protein complex. Negative stain electron microscopy and kinetic bioassays helped uncover structural and kinetic properties of this enzyme complex. With the assistance of a crosslinking reagent, the purified acyl-CoA carboxylase AccA3-AccD5-AccE5 was shown to be catalytically active *in vitro* but did not assemble into a complex that was viable for further imaging studies beyond negative stain electron microscopy screening. Possible explanations for this are discussed. Future studies could employ the use of substrate addition, more variables involved in the crosslinking procedure and increasing AccE5 expression levels in order to overcome limitations shown when attempting to achieve a stable complex. Further to this, we have demonstrated the potential for smaller complexes to be catalytically active which could have implications for future design of therapeutics, as shall be discussed.

1. Introduction

1.1 Mycobacterium tuberculosis

Mycobacterium tuberculosis (Mtb), the pathogen causing tuberculosis (TB), is recognized as a global health emergency by the World Health Organization (WHO) (Global Tuberculosis Report 2019, WHO). With an estimated global infection rate of 10 million new cases and 1.4 million deaths in 2017, TB is the leading cause of death from an infectious agent. About a quarter of the world's population are infected with *M. tuberculosis* and thus are at risk of developing the disease (Global Tuberculosis Report 2019, WHO). Drug-resistant TB remains a public health issue with 0.5 million new annual cases of rifampicin-resistant TB, 78% of which had multi-drug resistant (MDR) strains.

Socioeconomic decline, co-infection with human immunodeficiency virus (HIV), diagnostic delays and lack of adherence to complex treatment protocols in developing countries have exacerbated the problem. UN member states produced a political declaration, underlining the urgent need for new TB vaccines, treatments and diagnostic methods (UN Political Declaration, 2018). The prevalence of TB in developing countries such as Africa and parts of Asia is demonstrated in Figure.1.1.

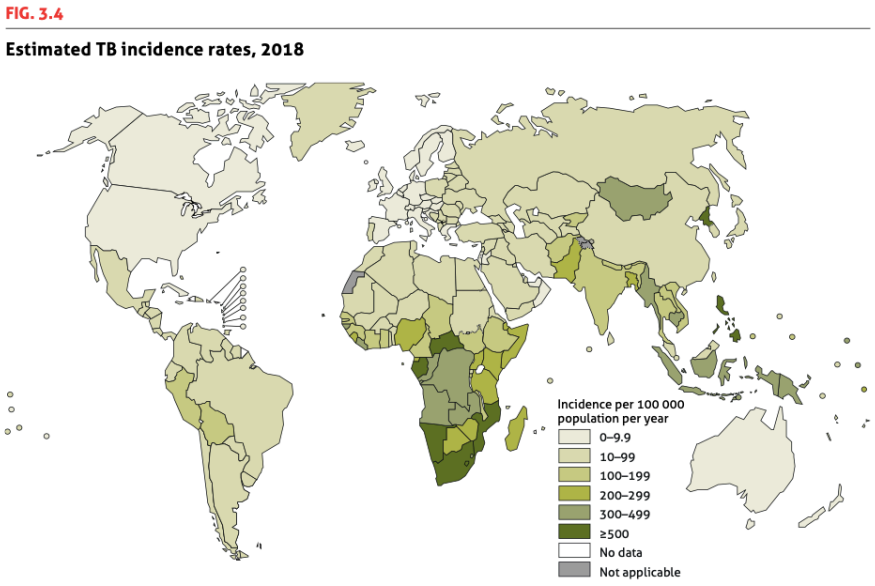

Figure 1.1: Incidence rate of *M. tuberculosis* per 100,000 (Global Tuberculosis Report 2019, WHO).

1.2 Transmission and Pathogenesis

Transmission

Studies on animal models and human TB have helped identify the pathway to which an organism becomes infected with *M. tuberculosis* (Flynn & Chan, 2005, Russell, 2007). Transmission is via airborne droplets from infected individuals containing one to a few bacteria that can pass the *M. tuberculosis* infection to others. These droplets are inhaled and deposit in lung alveoli. These are engulfed by alveolar macrophages, innate immune cells acting as the primary barrier against infection that most often kill the bacteria via phagocytosis. Bacterial contact with macrophage mannose or complement receptors can promote phagocytosis of *M. tuberculosis* bacteria (Schlesinger, 1993). Phagocytosed *M. tuberculosis* initially reside in an endocytic phagosome vacuole. Reactive oxygen species (ROS), acidic pH, lysosomal enzymes and antibacterial peptides kill most of the bacteria. However, some widespread strains of *M. tuberculosis* have evolved to be able to escape this first line of defence. This may be via preventing acidification of its surrounding environment (Crowle, *et al*., 1991). There is also evidence for bacteria inhibiting phagosome-lysosome fusion, thereby preventing the entry of lysosomal enzymes into its environment (Frehel, *et al.,* 1986).

Pathogenesis

Phagocytosis can result in the alveolar macrophages invading surrounding epithelial layers, giving rise to a localized inflammatory response that results in the recruitment of monocytes, lymphocytes and other immune cells (van Crevel, *et al.,* 2002). These act as host cells for the multiplying bacterial population and are not effective in reducing bacterial numbers. The mycobacterial ESX-1 type VII secretion system (T7SS) is required for the full virulence of Mtb, enabling translocation from phagosomes into the cytosol of infected macrophages. Here, *M. tuberculosis* may persist in a protected environment (Van der WN *et al*., 2007). The immune system attempts to control the infection by forming a granuloma structure, a collection of immune cells covered by fibrotic components that calcify the structure. This prevents further spread of bacteria due to the acidic pH

and low oxygen, but does not kill it (Dannenberg, 1994). *M. tuberculosis* cells within granulomas are considered metabolically quiescent, as characterized by limited or no replication and phenotypic resistance to drugs (O'Garra *et al*., 2013). This dormancy that can last for up to decades is called latent TB. This is asymptomatic and non-transmissible.

A weakened immune response due to altered antigen expression, imbalances in effector and regulatory T-cell or T-cell exhaustion, amongst other reasons, may allow TB to progress from latent to active. Characteristic of this is necrosis of the granuloma cells and a loss of granuloma vascularization (Russell, *et al*., 2009). Eventual rupture of the granuloma results in the release of many infectious cells into airways, spreading throughout the body via the lymphatic system and becoming transmissible as an aerosol via coughing or sneezing (Balasubramanian V *et al*., 1996, Kaplan, *et al*., 2003). This cycle can be seen in Figure. 1.2, with the final stage showing active TB.

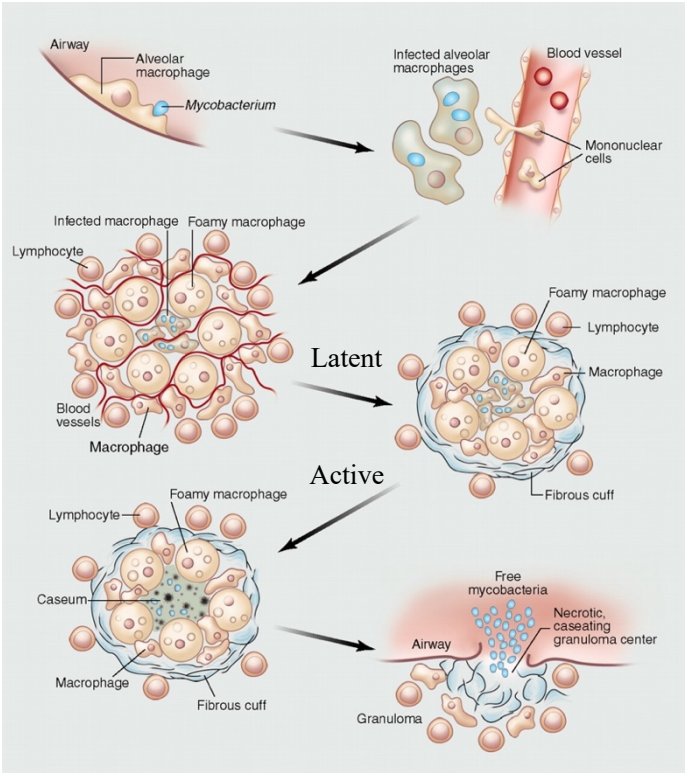

Figure 1.2: *M. tuberculosis* life cycle from initial infection of alveoli air sacs, to latent and active TB (Russel *et al*., 2010).

1.3 First and Second-line anti-TB therapies

The ability of *M. tuberculosis* to evade the host immunity has resulted in the need for antibiotics to fight or prevent disease. First line drugs (Table 1.1) are considered a standard set of treatments when someone is diagnosed with the disease. Second line drugs (Table 1.2) are used for MDR-TB. First-line anti-TB therapies are effective against non-resistant TB. However, a range of toxic side effects that differ between the drugs alongside the long treatment periods of several months can lead to incompletion of treatment and contribute to drug resistance (Salfullah *et al*., 2012). MDR-TB is resistant to at least RIF and INH (Table 1.1) and extremely drug-resistant TB (XDR-TB) is classified as MDR-TB with additional resistance to any fluoroquinolone and to at least one injectable second-line drug including capreomycin, kanamycin or amikacin (Table 1.2, Dalton, *et al*., 2012, Rendon *et al*., 2016).

Table 1.1: First line antibiotic drugs to treat *M. tuberculosis* infections.

Antibiotic	Target of inhibition	Reference
Streptomycin (SM)	Translation (16S rRNA of 30S ribosome)	Schatz *et al*., 1944
Isoniazid (INH)	Mycolic acid synthesis	Fox *et al*., 1952
Rifampin (RIF)	Transcription (RNA polymerase β-subunit)	Wehrli *et al.,* 1971
Pyrazinamide (PZA)	Coenzyme A, Ribosomal Protein S1	Malone *et al.,* 1952
Ethambutol (EMB)	Arabinogalactan synthesis	Shepherd *et al*., 1966

Second-line drugs are used for the treatment of those with drug-resistant TB. Typically, second-line drugs have higher toxicity, greater difficulty to procure and lower efficacy as they are designed

to be bacteriostatic (inhibit growth) rather than first-line drugs that are bactericidal (kill bacteria outright) (Rodrigo *et al*., 2006, Schaaf *et al*., 2016). Second-line drugs are divided into fluoroquinolones (Ofloxacin (OFX), levofloxacin (LEV), moxifloxacin (MOX) and ciprofloxacin (CIP)), injectable anti-TB drugs (kanamycin (KAN), amikacin (AMK) and capreomycin (CAP)) and others including ethionamide (ETH), cycloserin (CS) and P-aminosalicylic acid (PAS).

Table 1.2: Second line antibiotic drugs to treat *M. tuberculosis* infections.

Antibiotic	Target of inhibition	Reference
Fluoroquinolones	DNA Gyrase	Wright, *et al*., 2000
Kanamycin, amikacin, capreomycin	Protein Synthesis (16S rRNA)	Adamis, *et al.*, 2004, Blumberg, *et al.*, 2003
Ethionamide	Mycolic acid synthesis (enoyl reductase)	McIlleron, *et al.*, 2006
Cycloserin	Cell wall peptidoglycan synthesis (alanine racemase/ligase)	Wishart, *et al.*, 2006
P-aminosalicylic acid	Folate metabolism (dihydrofolate reductase)	Zheng *et al*., 2013

1.4 Novel anti-TB therapies and drug targets

Many first and second-line therapies are now known to be ineffective against some MDR-TB and XDR-TB strains. A range of new promising TB drugs currently in clinical trials are shown in Table 1.3. These next-generation compounds are the products of studies based around modern genetic approaches, compound screening and structural biology in order to identify anti-TB alternatives.

Table 1.3: Next generation anti-TB compounds currently in clinical trials.

Compound name	Clinical trial stage	New features	Reference
Moxifloxacin, gatifloxacin, Levofloxacin	III	Safer, shorter treatment duration	Cynamon*, et al.*, 2007, Lienhardt *et al*., 2016
Rifapentine	II	Serum half-life longer than RIF	Burman*, et al.*, 2001
SQ109	III	Activity higher than ethambutol	Jia, *et al.,* 2005
Bedaquiline (*Situro*^{TM})	II	Improved efficacy against resistant strains	Andries, *et al*., 2005
Sutezolid, Linezolid	II	Binds 23S ribosome to inhibit protein synthesis	Lienhardt *et al*., 2016
Q203	II	Blocks respiratory cytochrome bc_1 - lowers ATP production	Lienhardt *et al*., 2016

Novel drug targets

More recent TB drug discovery has generated hits with compounds that could progress to potential leads (Mdluli *et al*., 2014). These efforts are helping generate the next wave of TB drug target leads still in the preclinical phase, with some discussed below.

Iron is an essential nutrient for many living organisms, including pathogenic bacteria during an infection. During infection, *M. tuberculosis* localize inside host macrophages, where it can access transferrin-bound iron via secretion of mycobactins, molecules that can abstract iron from mammalian iron-binding proteins, allowing *M. tuberculosis* to internalize the iron (Kauffmann 2004, Rodriguez 2007). Mycobactin analogs that inhibited MbtA, the mycobactin biosynthesis enzyme, show superior activity to first-line TB therapies in preclinical trials (Neres *et al*., 2008).

Generation of reaction oxygen species (ROS) in the vicinity of a pathogen is hypothesized to be an essential feature of host immunity and antibiotics to enable bactericidal activity (Dwyer *et al*., 2009). The *M. tuberculosis* deazaflavin-dependent nitroreductase is hypothesized to provide protection from oxidative stress, with nitroreductase mutants being hypersensitive to some first-line therapies (Gurumurthy *et al*., 2013). Drugs that inhibit the nitroreductase activity may allow sufficiently high concentrations of ROS to accumulate and become bactericidal, without affecting host cells.

Another promising group of emerging targets are enzymes involved in lipid metabolism such as isocitrate lyase and fatty acid synthases (McKinney*, et al.*, 2000, Khasnobis*, et al.*, 2002, Nadav *et al*., 2018). Strongly related to this group of enzymes are those responsible for *M. tuberculosis* cell wall biosynthesis. Particularly relevant and unique to *M. tuberculosis* is the biosynthesis of mycolic acid components of the cell wall. Cell wall integrity is very important for *M. tuberculosis* survival, such as in unfavourable conditions in macrophage phagosomes and when subjected to antibiotics (Ma *et al*., 2001). Novel chemical compounds directed to inhibition of cell wall biosynthetic enzymes (enzyme components shown later in Table 1.4), could provide a powerful means to prevent bacterial infection in the host (Abrahams *et al*., 2018).

1.5 The cell wall of Mycobacterium tuberculosis

Mycobacteria are classified as gram-positive but possess features of gram-negative organisms too due to the unique chemical composition of the cell wall. Studies on the cell wall architecture identified lipids, glycans, pectins, mycolic acids and capsule-like material (Mudd*, et al.*, 1941, Goren 1972, Minnikin*, et al.*, 1982). A hallmark of the ability of mycobacteria to survive despite a fully functioning host immune system is the complexity of the cell envelope that is rich in structurally unique lipids and polysaccharides (Angala SK *et al*., 2014).

The cell wall is multi-layered, comprising a plasma membrane, peptidoglycans, arabinogalactans (arabinan and galactan pectins linked), mycolic acids and an outer capsule, as shown in Figure 1.3. Over 60% of the mycobacterial cell wall is lipid (Cole, *et al*., 1998). This hydrophobic structure provides protection against unfavourable conditions such as ROS, pH change, antibiotic entry and so is essential for cell survival (Briken*, et al.*, 2004, Hunter*, et al.*, 2006). *M. tuberculosis* has a large proportion (over 6%) of open reading frames (ORFs) encoding enzymes for fatty acid metabolism (Camus*, et al.*, 2002, Ehebauer &, 2011).

The cell membrane is composed of a thick outer layer and thin inner layer (Paul & Beveridge, 1992, Zuber, *et al.,* 2008). The outer layer contains phospholipids, carbohydrates and lipid anchors such as Lipid II to enable linkages to peptidoglycans in the cell wall core (Sibley, *et al*., 1988, Lemassu & Daffe, 1994, Guerardel, *et al*., 2002, Pitarque, *et al.,* 2008). The peptidoglycan layer is made of polymers of alternating N-acetylglucosamine and N-acetylmuramic acid residues, cross-linked by transpeptide bridges (Brennan *et al*., 1995) Peptidoglycan is unique to bacterial cells and acts to provide shape and rigidity, counteract turgor pressure and so is essential for growth and survival (Vollmer *et al*., 2008).

Arabinogalactan, a polysaccharide of arabinose and galactose sugar residues, is covalently linked to peptidoglycans by a single linker unit. This attachment is catalyzed by a GlcNAc-1-P transferase, rhamnosyltransferase and a Lcp1 ligase (Ishizaki *et al.,* 2013, Harrison *et* al., 2016).

Arabinogalactans function as attachment sites, signaling molecules and help define cell wall structures in all mycobacteria (Showalter *et al*., 2001).

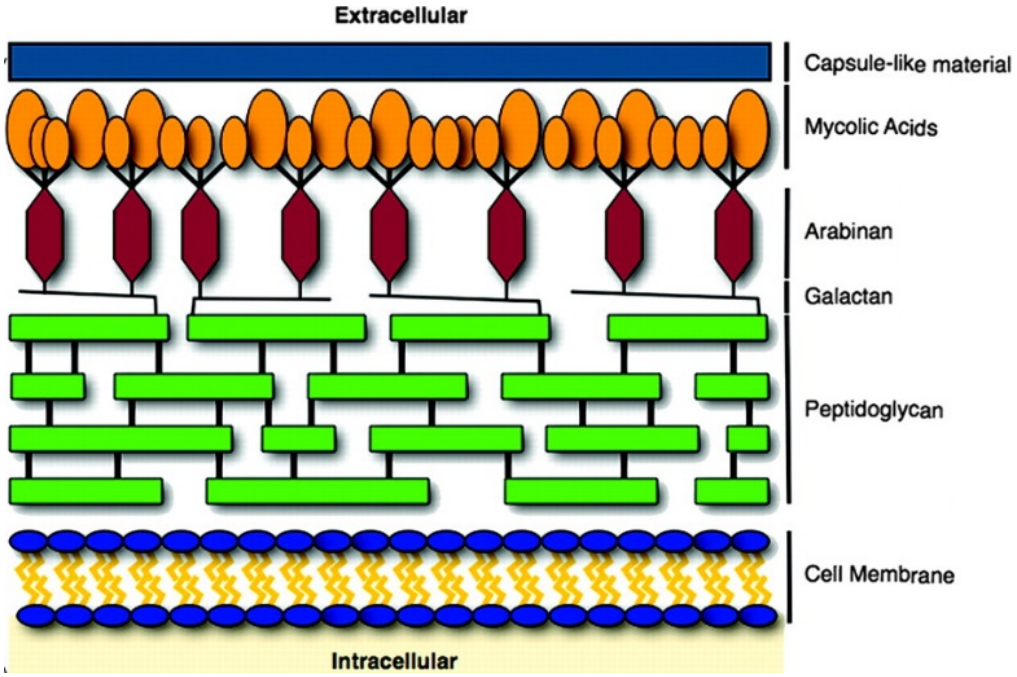

Figure 1.3: Diagram of the Mycobacterial cell wall, showing the basic intracellular to extracellular components including cell membrane (blue/yellow), peptidoglycans (green), galactans (black), arabinans (red), mycolic acids (orange) and capsule (blue).

The outer cell wall component is the capsule, primarily made of glycogen-like α-glucan, additionally with arabinomannans and mannans, proteins and lipids. Capsules are essential for bacterial cell wall integrity, commonly forming the outermost layer (Rainer *et al*., 2019). *M. tuberculosis* capsular components mediate interactions with macrophages to improve the likelihood of bacterial survival when exposed to the organism's immunity (Cywes *et al*., 1997).

The mycolic acid layer is a unique and essential component of the mycobacterial cell wall, linked to arabinogalactans via the non-reducing termini of the arabinan chains by the enzyme mycolyltransferase (David *et al*., 2007, Draper P *et al*., 1997). Mycolic acids are very long-chain α-alkyl, β-hydroxy fatty acids (Glickman, *et al.,* 2000, Vilcheze, *et al.,* 2000). Mycolic acids are synthesized by Fatty acid synthases I (FAS I), II (FAS II) and a polyketide synthase (Bhatt*, et al.,* 2005, Bhatt, *et al.,* 2007, Brown, *et al*., 2007). These fatty acids are essential for maintaining cell

wall architecture, limiting the effectiveness of hydrophilic antibiotics, provide resistance to chemical damage and dehydration (Liu J *et al*., 1996). They are the major component of the cell wall and are essential for mycobacterial growth and survival.

1.6 Fatty acid biosynthesis

Mycobacteria possess both fatty acid synthases I and II (FAS I/II). Other bacteria only harbor either FAS-I for *de novo* fatty acid biosynthesis as in corynebacteria and nocardia, or the multicomplex FAS-II for the elongation of existing medium-chain fatty acids which is the predominant synthase in prokaryotes (Harwood *et al*., 1988). Both types in mycobacteria exist, contributing to the unique lipid composition of the cell wall. This allows the generation of *de novo* fatty acids but also elongation of fatty acids to produce the meromycolate part of mycolic acids (Fernandes *et al*., 1996).

Mycobacterial FAS-1 synthases catalyze *de novo* synthesis of long-chain acyl CoAs C16:0 and C18:0 using acetyl-CoA and malonyl-CoA as the nucleating units respectively (Smith, *et al.,* 2003). These long-chain acyl CoAs have two paths they can take depending on the metabolic need of the bacteria as shown in Figure 1.4. They can be shuttled to the FAS-II system (pathway A) whereby C16:0 and C18:0 acyl-CoA units are condensed with malonyl-ACP to form 3-ketoacyl-ACP. This enters the FAS-II cycle to form acyl-ACP, involving the different FAS-II enzyme complexes mtFabH, MabA, HadABC and InhA as shown in Figure 1.4 (Carel *et al*., 2014).

Alternatively, C16:0 and C18:0 acyl-CoA units are subjected to additional elongation by FAS-I to produce a C26:0 acyl-CoA (pathway B) (McCarty *et al*., 1971). Pks13 polyketide synthase catalyzes the condensation reaction between acyl-ACP (from FAS-II) and C26:0 acyl-CoA (from FAS-I), converging the two pathways to produce α-alkyl β-ketoacids which are direct precursors of mycolic acids (Gavalda *et al*., 2014). The mycolic acid structure is shown.

The production of malonyl CoA by the enzyme acetyl-CoA carboxylase (ACC) is the first committed step in long-chain fatty acid and thus mycolic acid biosynthesis (Berg *et al*., 2002). This enzyme and related enzymes, such as propionyl-CoA carboxylases, are collectively known as acyl-CoA carboxylases (YCC) and are the focus of this study. Acyl-CoA carboxylases (YCC) are part of a larger family of enzymes called Biotin-dependent carboxylases.

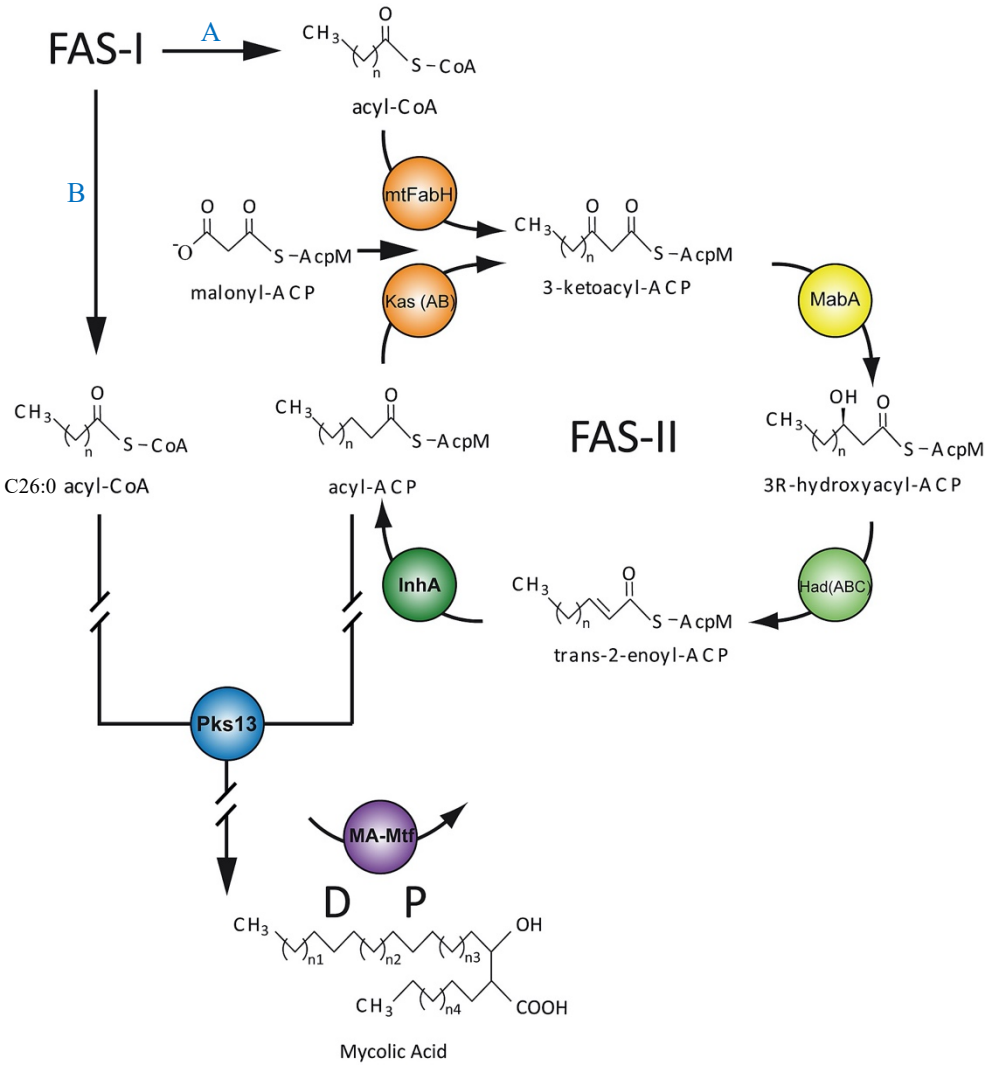

Figure 1.4: Diagram of the mycolic acid biosynthesis pathway

1.7 Biotin-dependent carboxylases

Biotin-dependent carboxylases

Biotin-dependent carboxylases include acyl-CoA carboxylases (YCC), 3-methylcrotonyl-CoA carboxylase (MCC), geranyl-CoA carboxylase, pyruvate carboxylase (PC), and urea carboxylase (UC) (Tong L., 2013). These enzymes have a diversity of functions including mycolic acid synthesis, terpenoid metabolism, carbohydrate metabolism, polyketide biosynthesis and urea utilization (Gago *et al*., 2011, Zhang *et al*., 2010, Forster *et al*., 2010, Navarathna *et al*., 2010). Most relevant to this study are YCCs as they are involved in the production of malonyl CoA and its derivatives as precursors for mycolic acid synthesis.

Mechanism of Biotin-dependent carboxylases

Biotin-dependent carboxylases have three structural components: biotin carboxylase (BC), biotin carboxyl carrier protein (BCCP) and carboxyltransferase (CT) (Gago *et al*., 2011). Biotin is covalently linked via an amide bond to a BCCP lysine side chain. There are two distinct enzymatic activities, catalyzing their reactions in two steps as seen in the reaction below in Figure 1.5.

The BC unit catalyzes the ATP-dependent carboxylation of the N1′ atom of the biotin cofactor, using bicarbonate as the carboxyl donor to form carboxybiotin (Knowles *et al*, 1989). This confers a conformational change in biotin attached to BCCP, allowing carboxybiotin to translocate from the BC active site to the CT active site (Knowles *et al*, 1989). In the second step, the CT component catalyzes the carboxyl group transfer from carboxybiotin to the substrate, forming a carboxyacyl-CoA product, e.g. malonyl-CoA.

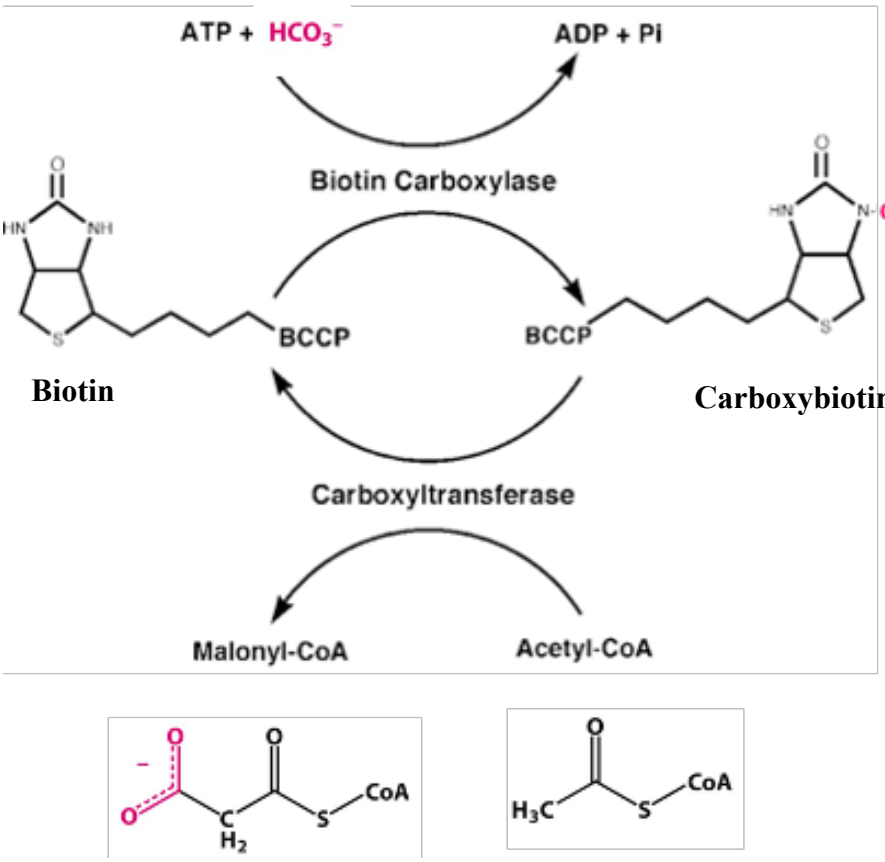

Figure 1.5: Diagram of the biotin-dependent mechanism for carboxyacyl-CoA production from acyl-CoA substrates.

1.8 Actinobacterial Acyl-CoA Carboxylases

Actinobacteria constitute one of the largest bacterial phyla. They are gram-positive bacteria with a high GC content in their DNA and a characteristic filamentous cell morphology (Dhakal *et al*., 2017). The three genera Mycobacterium, Streptomyces and Corynebacterium are well-studied as they are considered to be economically valuable for the production of bioactive secondary metabolites such as antibiotics, antitumour agents, immunosuppressive agents and enzymes. They can act as dangerous pathogens too e.g. *Mycobacterium tuberculosis, Streptomyces somaliensis* and *Corynebacterium diphtheria* (Berdy *et al*., 2005).

Roles of actinobacterial YCCs

Genome sequencing, biochemical analyses and structural biology has allowed the structural and functional characterisation of a number of YCCs from actinobacteria (Gande, et al., 2007, Gago, et al., 2006). In addition to malonyl-CoA for fatty acid biosynthesis, YCCs catalyse the carboxylation of propionyl-CoA, butyryl-CoA or long-chain acyl-CoAs to produce a diverse range of products for lipid and polyketide synthesis (Tran *et al*., 2015). In actinobacteria, the BC and BCCP together form the α-subunit. The CT is considered the β-subunit and demonstrates greater diversity, as shall be discussed.

Actinobacterial YCC subunit-encoding genes and functions associated were first illustrated in *Streptomyces coelicolor* (Diacovich, et al., 2002). The genome contained four genes for α-subunits (*accA1, accA2, pccA, SCO4381*), four genes for β-subunits (*accB*, PccB, SCO2776, SCO4380 and two for ε-subunits (*accE, PccE*) (Rodriguez & Gramajo, 1999, Rodriguez, et al., 2001). The genome of *Corynebacterium glutamicum* also carries genes encoding one α-subunit (*accBC*), four β-subunits (*accD1 – D4*) and an ε-subunit (a*ccE*) (Gande *et al*., 2007).

M. tuberculosis genomes encode genes for the YCC subunits: three α-subunits (*accA1-A3*), six β-subunits (*accD1-D6*) and an ε-subunit (*accE5*). The ε-subunit is proposed to help with the stability of some *accA-accD* complexes (Oh *et al*., 2006). YCC α-subunits (≈65kDa each) and β-subunits (≈60kDa each) complex in different combinations depending on the substrate. The structure is proposed to have α_6: β_6 subunits, with a stoichiometry of 1:1, making a dodecameric structure of approximately 750 kDa (Tong *et al*., 2017). This is supported by previously identified 750 kDa dodecameric forms of AccA1-AccD1 and AccA2-AccD2 (Ehebauer *et al*., 2015). Mutagenesis experiments in *M. tuberculosis* have shown *accA3* and *accA2* encode the α-subunits of the essential (critical to survival) YCC complexes in M. tuberculosis (Sassetti, et al., 2003, Griffin, et al., 2011). The different β-subunits are proposed to act on different fatty acyl-CoA units as substrates, conferring the ability to produce a highly diverse range of mycobacterial lipids (Ehebauer *et al*., 2015).

1.9 Mycobacterium tuberculosis Acyl-CoA carboxylases

The genome of M. tuberculosis encodes different YCC subunits. This range of β-subunits (AccD1-6) contribute to the diversity in lipid production for Mycobacteria. Different YCC complexes can form from the available subunits, with β-subunits showing specificity to different CoA substrates to produce lipid products as shown in Table 1.4 (Cole*, et al.*, 1998, Portevin*, et al.*, 2005, Gago*, et al.*, 2006). Some substrate interactions are yet to be characterised.

Table 1.4: Acyl CoA carboxylase subunits of *M. tuberculosis*

Subunit	**Protein**	**Active Expression**	**Substrate**
α-subunit	AccA1	Late log phase	Biotin
	AccA2	Late log phase	Biotin
	AccA3	Log phase	Biotin
β-subunit	AccD1	Late log phase	Methylcrotonyl-CoA
	AccD2	Late log phase	Unknown
	AccD3	Unknown	Unknown
	AccD4	Log phase	C_{26}-CoA
	AccD5	Log phase	C_3-CoA
	AccD6	Log phase	C_2-CoA
ε-subunit	AccE5	Log phase	None

The ability to form a range of functional YCC complexes has been demonstrated in a number of bait/prey pull-down experiments (Ehebauer *et al*., 2015). This helps to identify the 'interactome' as in Figure 1.6, which can act as a basis for further substrate identification and accelerate structural characterisation of complexes. Notably, AccA3 has a number of interactions with different β-subunits which can also interact with each other as well as AccE5 ('E' subunit). AccD3 does not

interact with any protein partners, with separate roles being suggested for this subunit due to low sequence similarity of <22% with other β-subunits (Ehebauer *et al*., 2015).

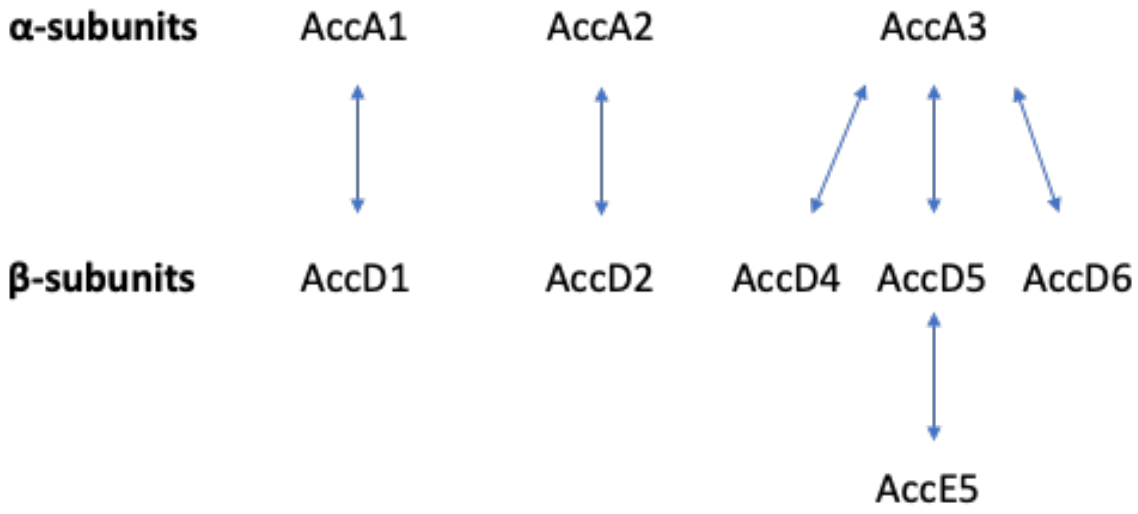

Figure 1.6: Diagram of the Acyl CoA carboxylase 'interactome', as identified by bait/prey experiments.

Mycobacterial YCC complexes involved in mycolic acid biosynthesis

The three YCC complexes that are identified to be involved in the mycolic acid biosynthesis pathway are AccA3-AccD4, AccA3-AccD5-AccE5 and AccA3-AccD6 (Gago *et al*., 2006, Kurth *et al*., 2009, Trivedi *et al*., 2004).

AccA3-AccD5-AccE5 complexes most likely generate methylmalonyl CoA for the biosynthesis of mycolic and other branched-chain fatty acids, due to its preference to utilise propionyl-CoA instead of acetyl CoA (Gago *et al*., 2006). Previous work on this complex includes the elucidation of the AccD5 crystal structure (Holton *et al*., 2006). In addition, biochemical experiments show complex activity is maximal in the presence of the AccE5 subunit (Gago *et al*., 2006). Structural characterisation of the complex could provide information critical to accelerate structure-based drug design.

AccA3-AccA6 generates malonyl CoA for mycolic and fatty acid biosynthesis, based on *accD6* mutagenesis experiments in *Mycobacterium smegmatis* (Kurth *et al*., 2009). The complex has also been shown to act on acetyl-CoA and propionyl-CoA substrates, with holoenzyme structures also yet to be characterised (Daniel *et al*., 2007).

AccA3-AccD4 is suggested to be involved in the generation of long-chain acyl carboxylic acids for the Claisen condensation reaction step in mycolic acid biosynthesis. This has been inferred from AccD4 orthologs only found in mycolic acid-producing bacteria, as well as *accD4* being in the proximity of genes *pks13* and *fadD32*, that encode a polyketide synthase and an acyl-AMP ligase involved in mycolic acid biosynthesis (Gago *et al*., 2011, Trivedi *et al*., 2004).

1.10 Aims of the study

The requirement of mycolic acids for the growth, survival and antibiotic resistance of Mycobacteria means the enzymes involved in mycolic acid synthesis are attractive potential drug targets. Acyl-CoA carboxylase complexes involved in this act at the rate-limiting step of mycolic acid synthesis. These complexes are essential to *M. tuberculosis* and have limited homology to similar enzymes in human beings. Despite being exciting potential drug targets, the AccA3-AccD5-AccE5, AccA3-AccD4 and AccA3-AccD6 complexes are yet to be structurally characterised.

This study intends to begin to structurally characterise the AccA3-AccD5-AccE5 complex using electron microscopy, alongside using a bioassay to provide kinetic analysis. This could help provide insights into the molecular structure and catalytic activity of ACCase in *M. tuberculosis*, thereby acting to assist structure-based drug design and additional future studies for other complexes involved in mycolic acid biosynthesis.

Experiments will initially be conducted using the non-native host *Escherichia coli* due to fast culture times and high expression potential to help gauge how we can optimise the expression and purification procedure using a near-native host to *M. tuberculosis*, this being *M. smegmatis*. Experiments will then be performed using the near-native host *M. smegmatis*, of which outcomes may be relatable to *M. tuberculosis* lipid metabolism and enzymes involved.

2. Materials and Methods

2.1 Materials

Consumables, chemicals and bacterial strains

A list of laboratory consumables used for the study are shown below in Table 2.1. These were obtained from a range of suppliers. Chemicals used were of analytical grade and purchased from Sigma-Aldrich, Merck Group and Carl Roth GmbH.

Table 2.1: Laboratory consumables used for the study

Consumable	Supplier
Centrifuge ultrafiltration filters	Merck
Chromatography columns	Bio-Rad
Cuvettes	Sarstedt
Electrophoresis gels	Biozol
Electroporation cuvettes	Biozym Scientific
Falcon tubes	Cellstar
Injection needles	B. Braun
Inoculation loops	Greiner Bio-One
Pipette tips	Sarstedt
Petri dishes	Sarstedt
Serological pipettes	Greiner Bio-One
Syringe filters	Sartorius
Syringe tubes	Henke Sass Wolf

E. coli and *M. smegmatis* strains used for cloning and expression were from the EMBL Hamburg bacterial strain collection. Different plasmid constructs containing genes encoding protein subunits and antibiotic resistance were cloned or expressed in these cells (see Appendix Table 6.2). *E. coli*

DH5-α cells were engineered to maximise transformation efficiency with three mutations recA1 to prevent heterologous recombination, endA1 for plasmid insertion and lacZM15 for blue-white colony screening (Kostylev *et al*.,2015). DH5-α were used for rapid cloning of pMyNt (Hygromycin-resistance, Addgene plasmid #42191) vectors which can then be isolated, transformed to *M. smegmatis* and expressed (Appendix). This uses *M. smegmatis groEL1ΔC* cells to purify poly-histidine tagged recombinant proteins. The genomes of these cells are deficient in a His-rich coding sequence of the Hsp60 chaperone GroEL1 to help with efficient expression and purification of only poly-histidine tagged target proteins without Hsp60 co-purifying (Noens *et al*., 2011).

Alternatively, BL21 *E. coli* cells that were engineered for expression directly in *E. coli* contain mutations, meaning they are deficient in proteases (Jeong *et al*., 2015). These were used for expression of pETM (Kanamycin-resistance) vectors. BL21 pRare cells are additionally deficient in RNAses but express additional tRNAs. The additional copies of certain rare codon tRNAs can assist protein production and stability for protein complexes, so as to prevent low abundance tRNA depletion and the subsequent failure to generate a full-length product that can otherwise occur in recombinant overexpression (Rosano *et al*., 2014, Pedersen, 1984). The incorporation of antibiotic resistance genes in a plasmid containing the desired gene to be expressed helps ensure only the bacteria that contain the desired gene are selected for to grow and reproduce (Diana *et al*., 2019).

Plasmid DNA isolation and purification

For the isolation of plasmid DNA from cloning *E. coli* cell lines, the QIAprep Spin Miniprep kit by Qiagen was used. Isolated plasmid concentrations were quantified using a Spectrophotometer to ensure sufficient yield (~ 5 mg plasmid per L culture) for our further transformation experiments into *M. smegmatis* (Liang *et al*., 2016).

The purification of proteins uses Superdex or Superose columns to conduct metal affinity chromatography of His-tagged proteins, followed by size exclusion chromatography (gel filtration) to isolate our target protein(s). Purified protein concentrations were also quantified using

a Spectrophotometer to ensure sufficient yield (~ 10 mg protein per mL culture) for our subsequent structural analysis experiments (Simonian, 2002).

2.2 Methods

Preparation of cloning and expression constructs

Prior to transforming plasmids into bacterial strains, genes of interest must be inserted into plasmids that contain antibiotic resistance genes. Initially, vectors were linearized and digested with restriction enzymes (RE) that cleave at specific cut sites to allow later gene insertion (Roberts, 2005). 2 µg of vector DNA was combined with 1.5 µL RE1 (e.g HindIII) + 1.5 µL RE2 (e.g. NcoI) + 3 µL NEB cutsmart buffer, totalling to 30 µL with the remainder being H_2O. This was incubated at 37 ºC overnight (~16 hrs). Linearized vectors will now have two ends containing phosphate groups that can re-circularize via ligation (Ukai *et al*., 2002). Therefore, the overnight protocol was followed by vector dephosphorylation using 3 µL of Antarctic phosphatase for 1 hour at 37 ºC (Maria *et al*., 2000).

Digested vector purification was conducted using a standard gel-purification technique. This uses an agarose DNA gel (0.5-2% agarose in distilled water) with a few drops (~10 µL each) of gel green (Sigma Aldrich). 6 µL DNA loading dye was combined with 30 µL vector and electrophoresed for 1 hour at 120 V. Gels were excised using a scalpel. To remove any contaminants a Monarch gel 'extraction' kit from New England Biolabs was used to yield a pure sample of digested vector DNA (Zhong, 2017).

Next, the gene of interest must be inserted into our digested vector. This was performed using a Seamless Ligation Cloning Extract ('SLiCE') Cloning Method (Zhang *et al*., 2014). The SLiCE extract was first thawed on ice and mixed well via vortexing. The mixture below was setup in a 0.5 mL microcentrifuge and mixed well via vortexing (Table 2.2). This was incubated at 37 ºC for 30-45min.

An aliquot of the plasmid vector with the insert were sent externally for DNA sequencing. Correctly inserted genes are now viable candidates for transformation into cells.

Table 2.2: SLiCE reaction mixture of components

Component	Amount
Purified Vector DNA fragment	50 - 200 ng
Purified Insert DNA fragment	Molar ratio insert: vector is 3:1
10X SLiCE Buffer	1 µL
PPY SLiCE extract	1 µL
MilliQ H_2O	Remainder to total 10 µL

Preparation of E. coli transformants

Chemically competent *E. coli* cells were prepared using the Inoue method (Inoue, *et al*., 1990). These cells were obtained from a previous EMBL researcher who details the method (Anandhakrishnan, 2013, Appendix).

E. coli cells used for transformation included DH5-α cells for cloning of pMyNt vectors, or BL21 cells for expression of pETM vectors. This uses a heat shock transformation protocol. A 100 µl frozen (-80 ºC) aliquot was thawed on ice. 1-2 µl plasmid DNA was gently mixed with the cells to create a mixture. This was incubated on ice for 30 minutes. Cells undergo a 42 ºC heat shock for 30-40 seconds and were immediately placed back on ice for 2 minutes. 400 µl of pre-warmed SOC medium was added to the mixture (Appendix) and incubated with shaking for 60min (37 ºC, 400 rpm). The transformation mixture was centrifuged (6,000 rpm, 2min), with the cell pellet being resuspended in SOC medium and plated onto an LB-agar plate, supplemented with the correct antibiotic(s) (Appendix). This was incubated at 37ºC overnight. Pre-cultures can be used for larger-scale expression procedures as will be described, or to create a stock of plasmid DNA. DNA stocks can be isolated using the 'QIAprep Spin Miniprep kit by Qiagen' kit (Olga *et al*., 2018). This only

requires small volumes (1-10 ml) of cell cultures, after which plasmid DNA can be quantified using a spectrophotometer and later frozen (-20 ºC).

Preparation of M. smegmatis transformants

All work with *M. smegmatis* was conducted in a laminar flow hood in a biological safety level 2 (S2) laboratory. These cells with the *groEL1ΔC* mutation were also obtained from a previous EMBL researcher (Anandhakrishnan, 2013, Appendix). Electrocompetent *M. smegmatis* cells are able to uptake exogenous genetic material after being subjected to an electrical field of a particular voltage i.e. electroporation (Goude *et al*., 2009).

For the transformation of *M. smegmatis* cells, a 100 µl frozen (-80 ºC) aliquot was thawed on ice. An electroporation cuvette was cooled on ice. 2-3 µl of plasmid DNA and 100 µl *M. smegmatis* cells were added to the electroporation cuvette. This reaction was incubated on ice for 20 min. Electroporation was performed at 2.7 kV twice. 500 µl of pre-warmed (37 ºC) 7H9 expression media was added to the cuvette and was mixed well (Appendix). The reaction mixture was transferred to an eppendorf tube and incubated at 37 ºC, 400 rpm for 1.5-2 hours. The mixture was centrifuged for 2min at 6000 rpm. The pellet was resuspended in the remaining media and plated onto a LB-agar plate, supplemented with the correct antibiotic(s), allowing growth to occur around 3-4 days later.

The pMyNt vectors cloned in *E. coli* were isolated and transformed into *M. smegmatis* - plated using Hygromycin (50 µg/ml) as the antibiotic. The full complex A3D5E5 was already present at the EMBL site in an *M. smegmatis* strain, as prepared by Sonja Staack. This has two plasmids co-expressed, with AccA3 (Kanamycin-resistance) on one plasmid and AccD5-AccE5 (Hygromycin-resistance) on another, both within the same cell. The vector map is shown in Figure 2.1.

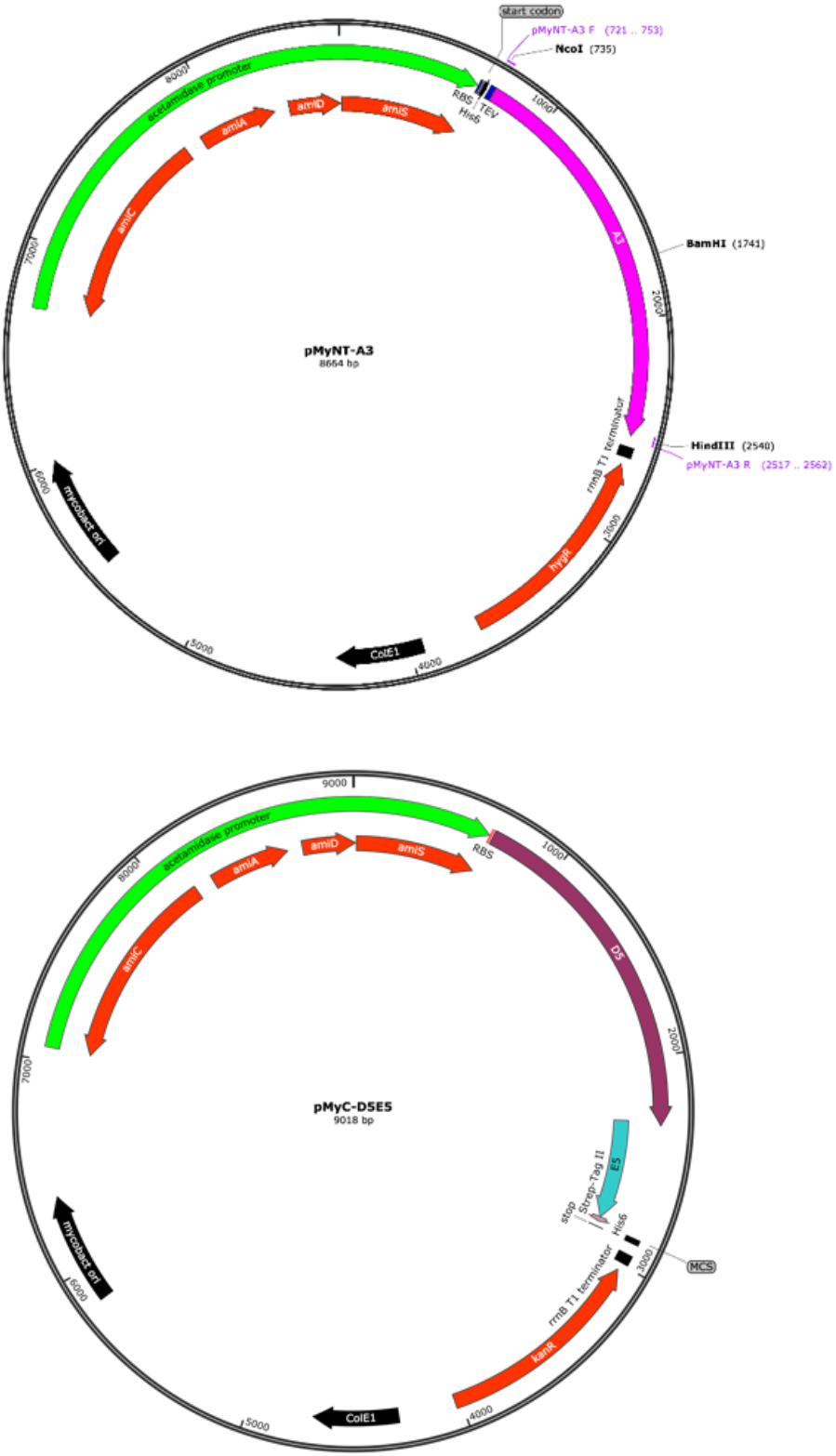

Figure 2.1: Vector map of the two plasmids expressing A3 and D5E5 in *M. smegmatis*

Large-scale protein expression in E. coli

For large-scale protein expression in bacteria, it is common to produce a pre-culture from agar-plate colonies to ensure growth, prior to scaling up. Scaling up is followed by protein expression induction and cell pellet harvesting.

100 ml LB media pre-cultures contain a single colony of cells, or an inoculation loop of cells from a glycerol stock, combined with the appropriate antibiotic(s) left overnight at 37 ºC, 150 rpm. 10-20 ml of the pre-culture was used to inoculate larger 1 L flasks of Terrific Broth (TB) media (47.6g TB powder and 4 mL glycerol dissolved in distilled water to a final volume 1 L.), supplemented with appropriate antibiotic(s) (Appendix). These cultures were incubated at 37 ºC, 150 rpm until an OD_{600} of 0.8-1 was reached. Here, induction of protein expression was via addition of IPTG at a final concentration of 0.1-0.5mM. Incubation continued for 4 hours at 37 ºC or for 16 hours at 18 ºC. Cells were harvested by centrifugation at 7,000 rpm for 30 min using a JLA 8.1000 rotor in an Avanti Centrifuge J20 XP (Beckman Coulter). Cell pellets were stored at -20 ºC until further use.

Large-scale protein expression in M. smegmatis

A 100 ml 7H9 expression media pre-culture contains a single colony of cells, or an inoculation loop of cells from a glycerol stock, combined with the appropriate antibiotic(s) left 3-4 days at 37 ºC, 150 rpm, as *M. smegmatis* takes longer to grow than *E. coli*. 10-20 ml of the pre-culture was used to inoculate larger 1 L flasks of 7H9 expression media, supplemented with appropriate antibiotic(s) (Appendix). These cultures were incubated at 37 ºC overnight, 150 rpm until an OD_{600} of 1-1.5 was reached. Here, induction of protein expression was via addition of 4.55 ml of 220X acetamide solution (Appendix). Acetamide upregulates gene expression by acting as an inducer at the promoter of the acetamidase operon, leading to downstream recombinant gene expression of Acc genes and subsequent protein expression (Sundararaman *et al*., 2014). Incubation was continued for 16 hours at 37 ºC. Cells were harvested by centrifugation at 6,000 rpm for 60 min using a JLA 8.1000 rotor in an Avanti Centrifuge J20 XP (Beckman Coulter). Cell pellets were stored at -20 ºC until further use.

Protein purification: Metal-affinity chromatography

Principle of metal-affinity purification

Proteins were purified from cellular contents using two techniques. This was using metal-affinity chromatography, followed by size exclusion chromatography (SEC). Metal-affinity chromatography is a well-known technique used to isolate a protein from a mixture of proteins and other cellular contents (Bornhorst *et al*., 2000). This utilizes the property of Histidine residues (His-tag) being able to bind divalent metal cations. Recombinant His-tag proteins contain a stretch of His residues that allow separation from non-tagged proteins in the cell lysate supernatant. The metal cation is Ni^{2+}, immobilized with Nitrilotriacetic acid (NTA) on the affinity column. After passing the cell lysate through the column, His-tagged protein will be bound to the Ni^{2+} ions. Detachment and elution of His-tagged protein was via addition of high imidazole concentrations, as imidazole outcompetes the His-tag to bind the Ni^{2+} cations (Bornhorst *et al*., 2000).

Protocol of metal-affinity purification

After large-scale protein expression, cells were thawed on ice and resuspended in lysis buffer (Appendix) with 1 mL DNAseI and 1 tablet of protease inhibitor cocktail added. *E. coli* cells were lysed by ultra-sonication. This used 3 x 3min cycles (0.5sec on + 0.5 sec off) with 2min pauses between sonication cycles. This uses a Bandelin Sonoplus sonicator with a VS 70T probe. Cell fractions were kept on ice during the sonication due to the heat that can be generated during this lysis procedure. Centrifugation of cells using a JA 25.50 rotor in an Avanti Centrifuge J20 XP (Beckman Coulter) at 19,000 rpm (20min, 4 ^{o}C) allows separation of cell lysate from protein that should be in the supernatant. Lysis of *M. smegmatis* cells utilize an Avestin EmulsiFlex-C3 High Pressure Homogeniser that applies pressure (20,000-25,000 psi) to lyse cells, generally re-applying the sample 3-4 times to ensure all cells were lysed (Uhlmann *et al*., 2013). Cell debris was removed via centrifugation (19,000 rpm, 90min, 4 ^{o}C) prior to purification.

Soluble cellular fractions (supernatant) were passed through a 0.45µm Sartorius syringe filter and loaded onto the Ni^{2+}-NTA resin column (5 mL HisTrap GE Healthcare column). Columns were

attached to an ÄKTA explorer protein purification system. Columns were washed and equilibrated using wash and binding buffers prior to imidazole addition (Appendix). Imidazole was added via the elution buffer (Appendix), with the final concentration increasing in a stepwise fashion (50 to 300 mM). The lower concentrations act to elute any loosely bound or contaminant proteins, followed by a linear high concentration of imidazole (300 mM) addition to elute our target protein. Here, our recombinant protein should elute into fractions for SDS-PAGE analysis, as will be detailed. All purification steps were carried out at 4 ºC to help minimize protein stability issues.

Protein purification: Size-exclusion chromatography

Principle of SEC

SEC aims to separate molecules based on their size (hydrodynamic radius) (La Verde *et al*., 2017). The chromatography column contains fine, porous beads made of either polyacrylamide, agarose or dextran polymers. Different sized molecules migrate at different rates through the column, with smaller beads migrating slower as they are more likely to enter the pores, whereas larger molecules elute first as they are less likely to enter these pores (La Verde *et al*., 2017). A larger volume of SEC buffer must be applied to elute the smaller molecules (Appendix).

Protocol of SEC

Proteins obtained via affinity chromatography were checked on an SDS-PAGE gel to ensure there was sufficient protein expression and purity of our recombinant protein(s). Proteins were loaded onto a column via sample injection into an ÄKTA explorer protein purification system (uses a Superose TM 6 GE Healthcare column). This was washed and equilibrated using wash and SEC buffers (Appendix). Eluted proteins were analysed on chromatograms and collected in designated fractions for SDS-PAGE analysis. In some cases, affinity tags e.g. SUMO were removed via TEV protease addition overnight (4 ºC). Tags such as SUMO can help with identifying the protein or initiate cellular processes such as protein expression and folding (Peroutka *et al*., 2011).

Gel electrophoresis

Gel electrophoresis allows the separation and analysis of macromolecules based on their size and charge (Ames, 1974). Proteins can migrate on polyacrylamide (PAGE) gel substrates when exposed to an electric field, with their size and charge determining the rate of migration. This separation technique is useful for analysing the biochemical purity of samples after affinity or size exclusion chromatography. Addition of anionic Sodium dodecyl sulfate (SDS) detergent to a protein imparts a total negative charge on the protein(s). SDS masks the charge of amino acid side chains, meaning migration is now determined by size from positive to negative electrodes i.e. the larger the size, the shorter the migration distance (Costas, 1995). Beta-mercaptoethanol (β-ME) is also added to assist with denaturation by reducing disulphide bonds (Kartheek *et al*., 2019).

Samples were combined with a Biolabs purple gel loading dye (15 µl sample, 5 µl dye). Mixing by brief centrifugation was followed by heating of samples (75 ^{o}C, 10min) and β-ME addition (5% w/v sample) to denature any secondary, tertiary or quaternary structures to allow separation of individual proteins. These denatures samples were loaded onto the 'Mini-Protean Tetra Cell' vertical protein electrophoresis system (Bio-Rad), using a Biozol expedeon 12 or 17-well gel. This system uses an NuPAGE MES SDS running buffer (151.4g Tris base, 720g Glycine, 50g SDS and distilled water up to a 5 L solution). A pre-stained 'PageRuler' protein ladder was also loaded to estimate molecular weight (kDa) of loaded protein samples. Samples were electrophoresed for 45-60min at 160-180V. Gels were washed with ddH_2O and stained using the Coomassie blue stain (0.8g Brilliant blue G-250 is added to 500 mL distilled water and dissolved with stirring overnight at 4 ^{o}C. 34mL of 32% (v/v) HCl is added and the volume was made to 1000 mL with distilled water). Gels were destained with ddH_2O and imaged using Coomassie fluorescence detection.

Native gel electrophoresis uses commercial pre-cast gels with 10 wells and a non-SDS containing buffer with high Coomassie Brilliant blue concentrations (increased concentrations (0.2-5%) of Brilliant Blue G-250 were made for running Native gels). For this study, complex size can be estimated using this method after performing size exclusion experiments. The Coomassie dye coats

the protein in a negative charge similar to SDS. However, this is not denaturing and so complexes migrate based on their intact size (Wittig *et al*., 2010). Gels were run using a combination of protein and Thermo Scientific™ Pierce™ Lane Marker Sample Buffers (15 µl sample, 5 µl dye). SDS and heating of samples were not required for this technique as we want to keep the complex intact. Samples were electrophoresed for 3 hours at 150-200V, ensuring >5mA was maintained for proper migration. Samples were then de-stained for 3-4 days using a de-staining solution (Native de-staining solutions were made with 20% (v/v) ethanol, 5% acetic acid (v/v) and 1% glycerol (w/v) in 500 mL distilled water. This was stored at 4 ^{o}C.).

Centrifugal ultrafiltration and measuring protein concentration

Protein samples were concentrated using centrifugal ultrafiltration (4000 rpm, 4 ^{o}C) in a time-dependent manner i.e. the longer ultrafiltration time, the more concentrated the protein (Blanco *et al*., 2004). This used a 100kDa filter as complexes were estimated to be around 140kDa. Estimating protein concentration was performed using a NanoDrop Spectrophotometer (PEQLAB) that measures light absorption at UV_{280nm}. This uses the principle of the Beer-Lambert Law (Beer, 1852). The law demonstrates the relationship between absorbance (A), molar concentration (c, M) with the path length of light (L, cm), the and the molar extinction coefficient (Ɛ, $M^{-1}cm^{-1}$). The molar extinction coefficient can be calculated using online softwares (expasy.org) to multiply the total extinction coefficients of absorbing species (Tyr, Trp, Cys disulphides) by their number per protein molecule. The law is shown in the equation below:

$$C = \frac{A}{\text{Ɛ} * \text{L}}$$

Crosslinking protein subunits

Some protein complexes may be unstable after purifying as they are stored in non-native conditions. Attempts to maintain stability can be performed using crosslinking techniques. Crosslinking may be necessary for subunits with low *in vitro* binding affinity and is a relatively simple procedure. Buffers used for purification steps involving crosslinking proteins have Tris-

HCl replaced with HEPES to prevent Tris-HCl quenching the glutaraldehyde during the purification. After size exclusion purification of protein subunits, samples should be concentrated using centrifugal ultrafiltration to around 1 mg/mL. Proteins were then mixed with the glutaraldehyde (GA) crosslinking agent at a range of final concentrations, typically 0.01-0.1% of GA.

This reaction was incubated on ice for 1 hour and quenched by addition of 40mM (final concentration) of Tris-HCl to prevent further crosslinking. Samples were run on an SDS-PAGE or native gel alongside non-crosslinked controls to show if the crosslinking was effective. Here, the optimal crosslinker concentration and incubation time can be identified before further purification or imaging studies. The crosslinking mechanism is shown below in Figure 2.2, with aldehyde groups of GA binding to amine groups of proteins to help form inter-particle crosslinks. GA is the carbonyl reagent that condenses amines via Mannich reactions or reductive amination (Bala *et al*., 2014).

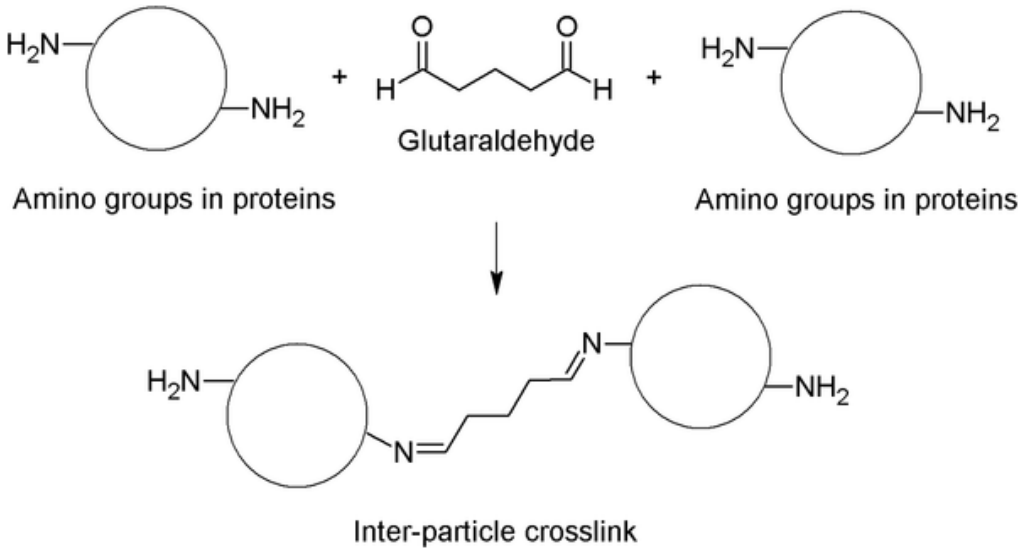

Figure 2.2: Crosslinking mechanism of glutaraldehyde (Thongnuanchan *et al*. 2018).

Electron Microscopy

Principle of EM

Electron microscopy (EM) is a useful screening tool to identify the optimal protein concentration for imaging and whether or not the protein complex would have a resolvable structure during crystallisation trials or Cryo-EM studies. EM uses a beam of accelerated electrons typically from a tungsten cathode electron gun to illuminate the sample. This achieves a higher resolution than that of light microscopes, the resolution of which is limited by the longer wavelength of photons compared to electrons (De Haan *et al*., 2019). The signals scattered or emitted from the sample are measured on a detector or camera that allow construction of a sample image. Two common types of EM are scanning EM (SEM) and transmission EM (TEM). SEM scans with electrons along a series of rectangular areas of a specimen, giving information on sample surface topography and composition. TEM uses thin sections of specimens placed on a grid. TEM beams are transmitted through the sample with the image magnified and captured, typically onto a fluorescent screen or photographic film. TEM utilizes a shorter wavelength (higher acceleration voltage (kV)) of electrons to deliver a higher resolution than SEM (Bogner *et al*., 2007).

Sample complex stability and purity can be screened using negative staining TEM. Negative stain studies used a thin specimen contrasted with an optically opaque salt such as uranyl acetate or ammonium molybdate (Scarff *et al*., 2018). The fluid stains the background, meaning the specimen remains untouched, light and visible contrasted to the darker background. The background comprises small particles that can bind to the staining fluid, a fluid that scatters electrons strongly compared to the protein sample (Scarff *et al*., 2018). This results in background particles appearing dark and invisible in contrast to the lighter, visible sample. Prior to sample application, the carbon-coated copper grids (300 mesh, ScienceServices) loaded into EM machines were glow-discharged. Glow-discharge applies an electric current in the form of plasma for up to 120s. This removes any contaminant particles on the grid surface and makes the surface hydrophilic to encourage sample adherence (Gallagher *et al*., 2019). Samples and stains are applied in μL volumes to carbon-coated copper grids prior to imaging.

Protocol of sample preparation and EM imaging

In order for resolution of individual particles, samples must have a concentration of approximately 0.1 mg/mL using centrifugal ultrafiltration, as measured via the NanoDrop Spectrophotometer. Samples were kept on ice prior to being applied to individual grids. Initially, the grids were glow-discharged and held by tweezers to make sample application easier. 20 µL buffer (normally SEC buffer from the most recent purification) is pipetted to wash the grids and this was blotted using clean paper after 30 seconds to remove liquid. After this, 20 µL of the sample protein was added and fixed for 30 seconds. This was followed by addition of 15 µL of uranyl acetate (2%, dissolved in distilled water) addition to the grid. 30 seconds later, this mixture was blotted to remove any liquid. Liquid must be removed as the EM sample stage must maintain a vacuum.

Grids were loaded into the EM, with the sample loading area kept cool by a liquid nitrogen source. Images were taken using a range of adjustments to the magnification and focus as appropriate. Images should be taken from a sample of regions on the grid for a representative set of images. If the sample protein can be resolved, 1000s of 2-D images can be taken automatically of similar structures to give a single-class average image of the protein of interest (Qi *et al*., 2017).

Kinetic characterisation of protein complexes

Demonstration of *in vitro* catalytic activity would be complementary to purification and imaging studies in order to show an active complex is present and the activity is intact. Complex enzymatic activity can be measured using biochemical assays.

Kinetic model

Michaelis-Menten kinetics, a simple and popular choice to model an enzyme's activity, assumes a reaction between a substrate and enzyme to help identify a number of kinetic constants relating to the complex (Michaelis *et al*., 1913). The hyperbolic model is based on the hypothesis that the rate-limiting step in enzymatic reactions is the breakdown of enzyme-substrate complexes to

product and free enzyme, with an eventual saturation of enzyme activity upon substrate addition (Michaelis *et al*., 1913).

Typically, a reaction is setup involving the enzyme at a constant concentration and substrate(s) added at varying concentrations [S]. The reaction rate (v) can be measured via measurable product formation from the reaction. From this, we can interpret the V_{max} which represents the maximum rate of product formation achieved in our system, and the K_M which is equal to the substrate concentration required to reach half of V_{max} (Michaelis *et al*., 1913). The equation for the kinetic model can be seen below.

$$v = \frac{Vmax\ [S]}{Km + [S]} \quad \text{(µmol/min)}$$

Acyl-CoA Carboxylase assay

Carboxylase activity of AccA3-AccD5 complexes can be estimated using an enzyme-coupled assay (Sausen *et al*., 2019). This assay follows the rate of NADH oxidation spectrophotometrically as a proxy of ATP hydrolysis by the carboxylase complex as shown in Figure 2.3. The assay was previously optimised to ensure the ACCase step was the rate-limiting component (Anandhakrishnan, 2013).

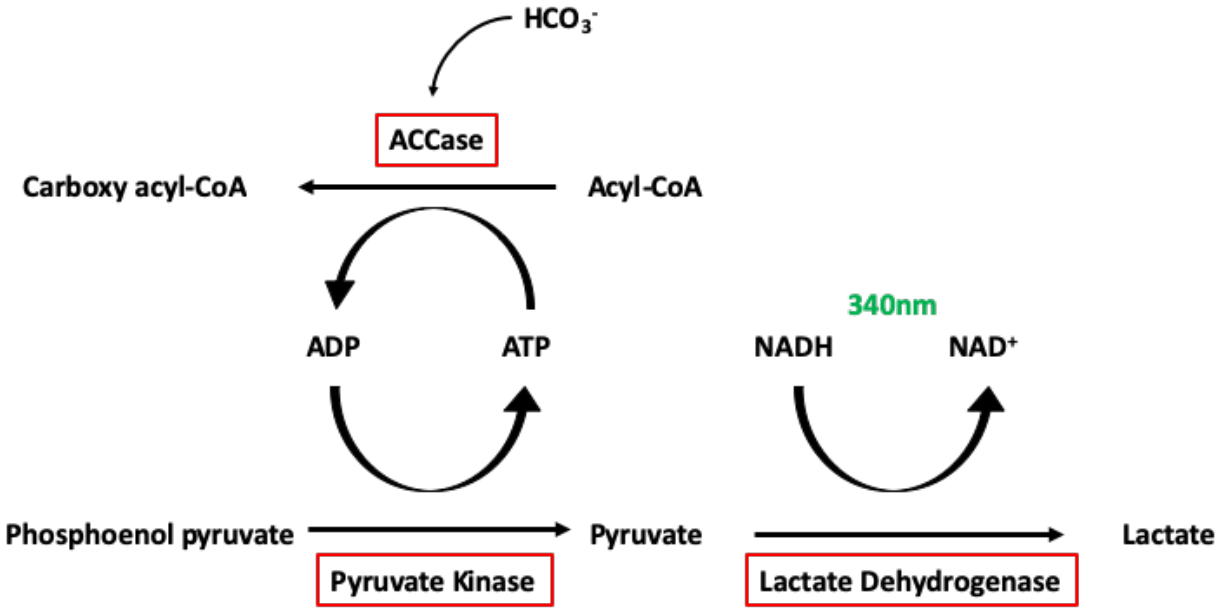

Figure 2.3: Enzyme assay used to measure the catalytic activity of Acyl-CoA Carboxylases. Activity is measured spectrophotometrically via the oxidation of NADH during Lactate formation.

Acyl-CoA Carboxylase complexes utilize ATP, with ADP as a by-product. ADP can be phosphorylated in the reaction catalysed by pyruvate kinase to form pyruvate. Activity of this reaction was measured via the absorbance of the NADH metabolite. NADH in solution produces a significant absorbance peak at 340 nm, while NAD^+ has low to no absorbance at this wavelength but has a peak at 260nm (Sausen *et al*., 2019). This assay is hypothesised to measure NADH oxidation at 340nm upon substrate addition, as this is indicative of the rate of ATP hydrolysis (Sausen *et al*., 2019). Therefore, the rate of reaction (v) can be calculated from rate of NADH oxidation to NAD^+, as measured by the changes in absorbance of NADH at A_{340nm}.

As with previous kinetic trials, the assay mixture (components from Sigma) contains: 7 units of pyruvate kinase, 10 units of lactate dehydrogenase, 50 mM $NaHCO_3$, 3 mM ATP, 0.5 mM phosphoenol pyruvate, 0.2 mM NADH, 0.3 mg/ml BSA, 100 mM K_2HPO_4 and 5 mM $MgCl_2$ and varying concentrations of Acyl-CoA substrate. This is conducted at pH 7.6, with enzyme units (U) being defined as amount of the enzyme that catalyses the conversion of 1 µmol substrate to product per minute (typically at 25 ^oC).

Reactions were initiated by the addition of the Acyl-CoA Carboxylase to the assay mixture (Appendix) and kept at 30 °C. Absorbance data were acquired using a multimode microplate reader (Infinite M1000, Tecan) at A_{340nm} which were used to calculate the rate of product formation (µmol/min). The K_m and V_{max} were determined by fitting the rates of reaction against the substrate concentration.

3. Results

3.1 Protein Purification and Imaging of E. coli ACCase

Expression and Purification of E. coli AccA3-AccD5-AccE5

Affinity Chromatography

The requirement of mycolic acids for the growth, survival and antibiotic resistance of Mycobacteria means the enzymes involved in mycolic acid synthesis are attractive potential drug targets. Acyl-CoA carboxylase complexes involved in this act at the rate-limiting step of mycolic acid synthesis. Despite being exciting potential drug targets, the AccA3-AccD5-AccE5, AccA3-AccD4 and AccA3-AccD6 complexes are yet to be well-characterised. The purification steps intend to obtain a high purity protein sample from *M. smegmatis* that can be used for structural and kinetic characterisation. This process could help provide insights into the molecular structure and catalytic activity of ACCase in *M. tuberculosis*.

After successful cloning and transformation of plasmids into the chosen host, AccA3, AccD5 and AccE5 were separately expressed in *E. coli*. Protein overexpression was induced, and cells were harvested after incubation. Three separate affinity chromatography runs allowed isolation of the individual proteins from the supernatant of centrifuged mixtures, yielding ~25 mL of protein-containing fractions at concentrations of ~2 mg/mL.

As explained in the Methods section, the use of the *E. coli* pRare strain was chosen as a non-native host for the production of AccA3 and AccD5 proteins (Anandhakrishnan, 2013). The affinity chromatograms and SDS gels are shown below in figures 3.1A-F.

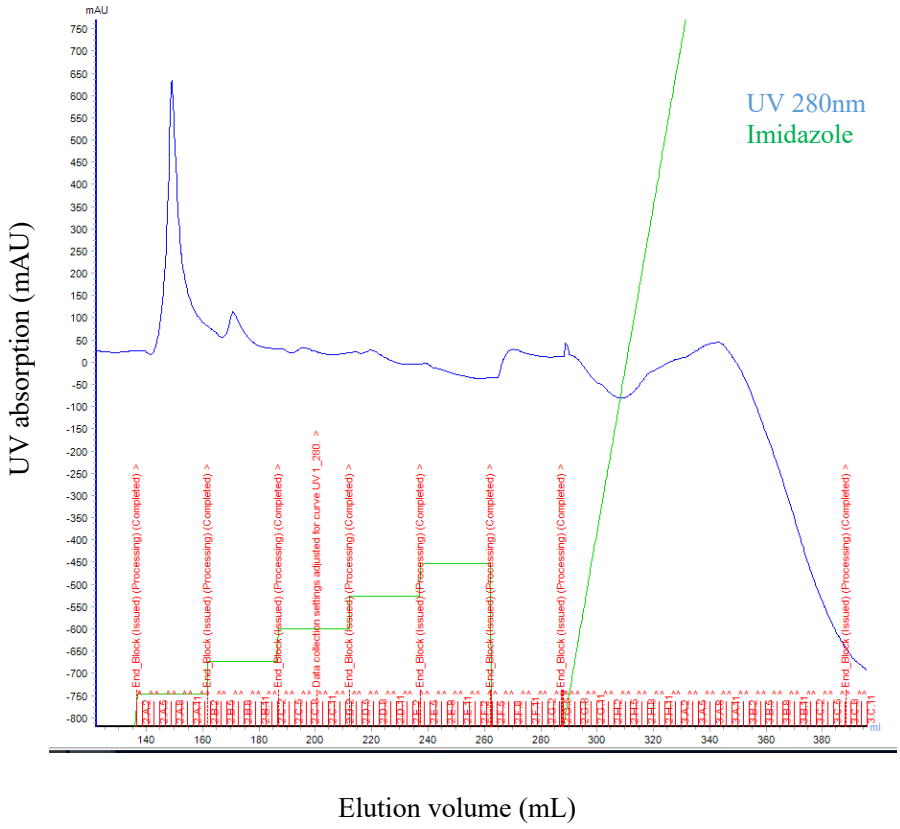

Figure 3.1A: Affinity chromatogram of AccA3. Imidazole addition is shown in green on the chromatogram in a stepwise and linear manner. His-tagged protein is eluted into fractions 2H2-3C11 (only raw data was available for this chromatogram).

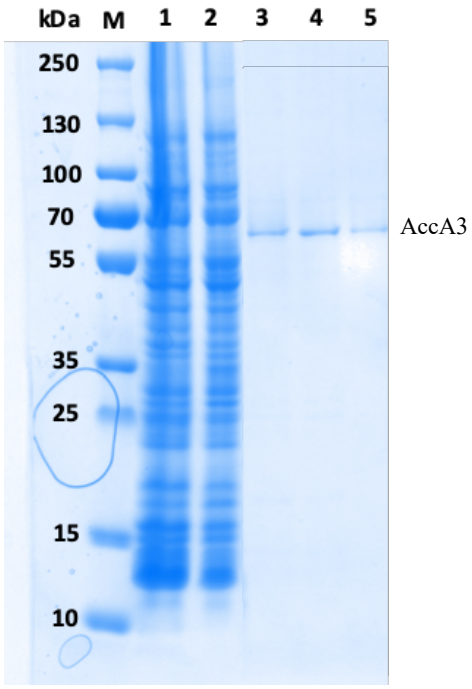

Figure 3.1B: SDS-PAGE gel of AccA3. Lanes 1 and 2 are non-purified supernatant and HisTrap flow through respectively. Eluted in lanes 3, 4 and 5 is the AccA3 protein, estimated to be 64kDa.

Figures 3.1A plots the elution volume (ml) against the UV absorption (mAU) of the eluted AccA3 sample. A stepwise addition of imidazole at 6, 12, 24 and 48 mM is shown to remove any loosely bound contaminant particles from the column. This was also used in case our protein elutes at low imidazole concentrations, allowing us to optimise the elution process. This is followed by a linear addition of imidazole from 0-300 mM to completely elute our target His-tagged protein. Fractions where our His-tagged protein elutes were run on an SDS PAGE gel, shown in figure 3.1B. The AccA3 protein size is approximately 64kDa, as calculated from the marker protein ladder in lane M. The molecular weight of purified AccA3 is consistent with prior Expasy sequence analysis.

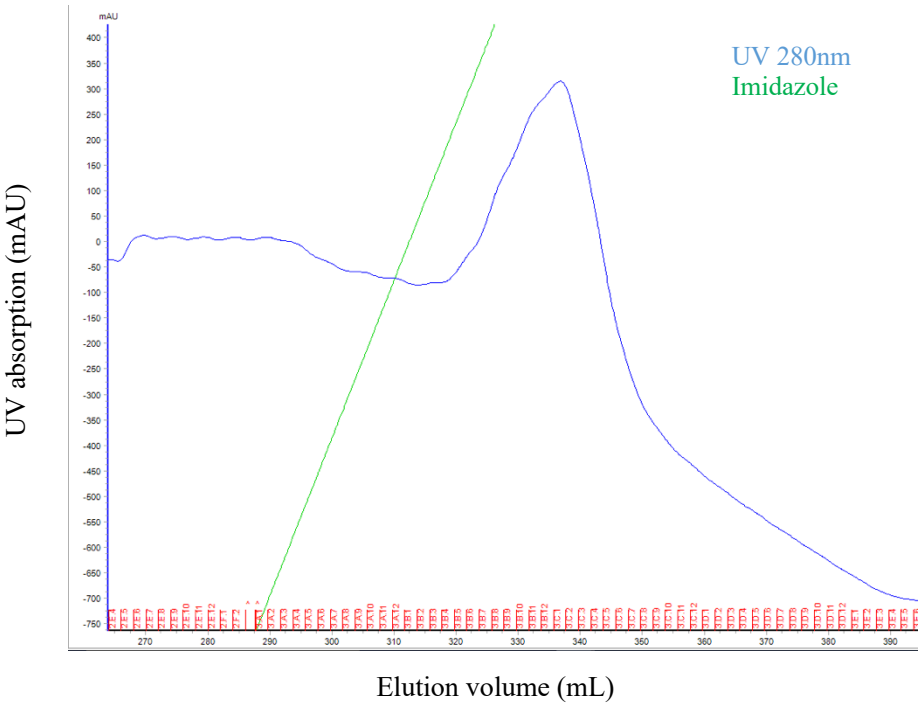

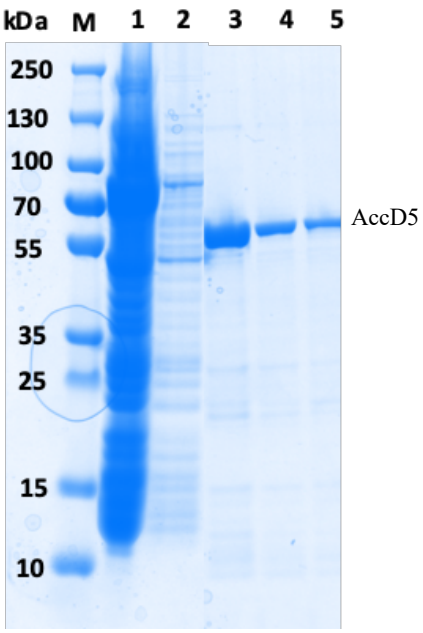

Figure 3.1C: Affinity chromatogram of AccD5. Imidazole addition is shown in green on the chromatogram with the linear addition shown. His-tagged protein is eluted into fractions 3B4-3E3.

Figure 3.1D: SDS-PAGE gel of AccD5. Lanes 1 and 2 are non-purified supernatant and HisTrap flow through respectively. Eluted in lanes 3, 4 and 5 is the AccD5 protein, estimated to be 59kDa.

Figures 3.1C plots the elution volume (ml) against the UV absorption (mAU) of the eluted AccD5 sample. Again, there is a stepwise addition of imidazole at 6, 12, 24 and 48 mM is shown to remove any loosely bound contaminant particles from the column, followed by a linear addition of imidazole from 0-300 mM to completely elute our target His-tagged protein. Fractions where our His-tagged protein elutes can be used for an SDS PAGE gel, shown in figure 3.1D. The AccD5 protein size is approximately 59kDa, as calculated from the marker protein ladder in lane M. The molecular weight of purified AccD5 is consistent with prior Expasy sequence analysis. AccD5 shows a similar gel profile to AccA3, but with a higher concentration.

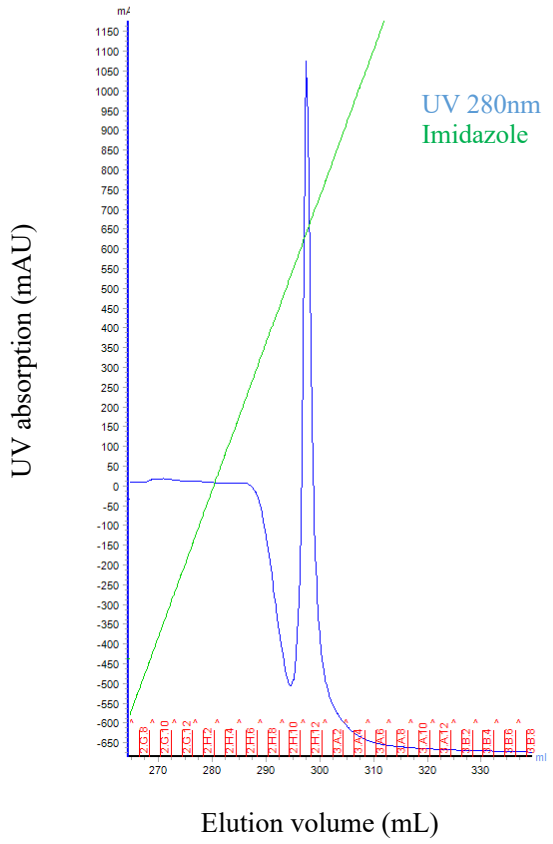

Figure 3.1E: Affinity chromatogram of AccE5. Imidazole addition is shown in green on the chromatogram with linear additions shown. His-tagged protein is eluted into fractions 2H9-3A2.

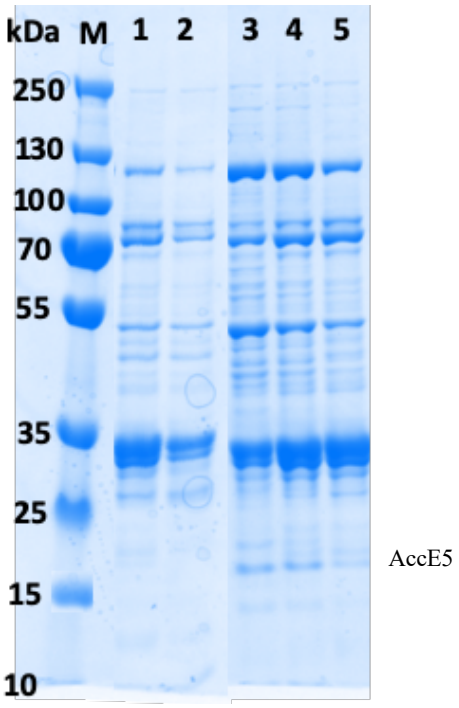

Figure 3.1F: SDS-PAGE gel of AccE5. Lanes 1 and 2 are non-purified supernatant and HisTrap flow through respectively. Eluted in lanes 3, 4 and 5 is the AccE5 protein estimated to be 19kDa.

Figures 3.1E plots the elution volume (ml) against the UV absorption (mAU) of the eluted AccE5 sample. Again, there is a stepwise addition of imidazole, followed by a linear addition of imidazole to elute our target His-tagged protein. Fractions where our His-tagged protein elutes can be used for an SDS PAGE gel, shown in figure 3.1F. The AccE5 protein size is approximately 19kDa, as calculated from the marker protein ladder in lane M. After several repetitions of this experiment using appropriate equipment washing procedures, the samples were proving difficult to purify without contamination. Further to this, the proposed AccE5 observed on the gel eluted at a low concentration and appeared slightly larger in molecular weight compared to prior Expasy sequence analysis.

Crosslinking and Imaging of E. coli AccA3-AccD5-AccE5

Crosslinking E. coli ACCase components

Previous optimisation experiments showed that we required additional crosslinking agents to maintain protein complex stability for further imaging and kinetic analysis of the ACCase subunits, the rationale for which has been explained previously. Some protein complexes may be unstable after purifying as they are stored in non-native conditions. To generate improved complex stability for EM imaging, crosslinking the components was utilised. Samples AccA3, AccD5 and AccE5 were optimised for crosslinking at a concentration of 1 mg/ml and mixed in equal volumes prior to crosslinking. Samples separated on an SDS gel are shown below in figure 3.1G. The optimal crosslink concentration range must now be identified using a combination of SEC and a native gel.

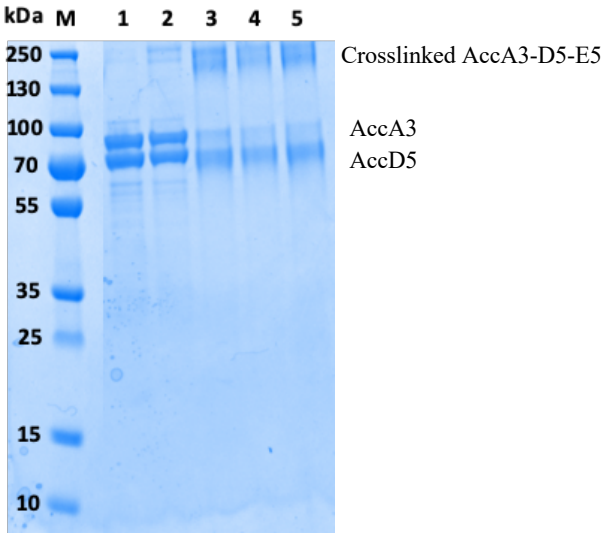

Figure 3.1G: SDS-PAGE gel of crosslinked AccA3-D5-E5 components from *E. coli*. Lane 1 shows a non-crosslinked AccA3-D5-E5 sample. Lanes 2-5 show crosslinker added to the sample at 0.01, 0.02, 0.05 and 0.1% respectively.

Size Exclusion Chromatography

All crosslinked samples from the HisTrap study were optimised for SEC to a concentration of 0.05 mg/mL. As an example, figure 3.1H shows the SEC elution profile of 0.1% GA addition to our

sample. The elution profile suggests presence of a heterogeneous sample. Figure 3.1I shows the native gel of SEC samples with crosslinker added to our sample at a range of concentrations.

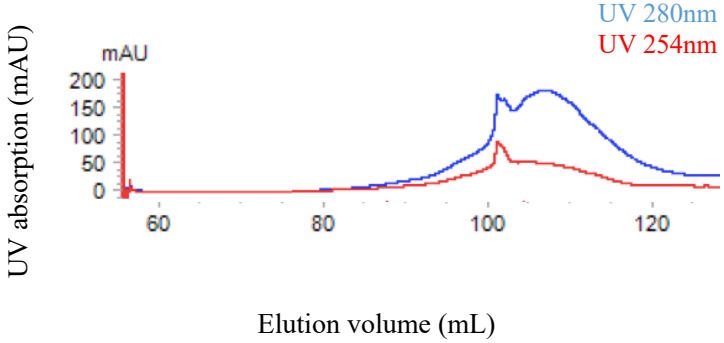

Figure 3.1H: Size exclusion profile of AccA3-D5-E5 complex using 0.1% GA crosslinker addition

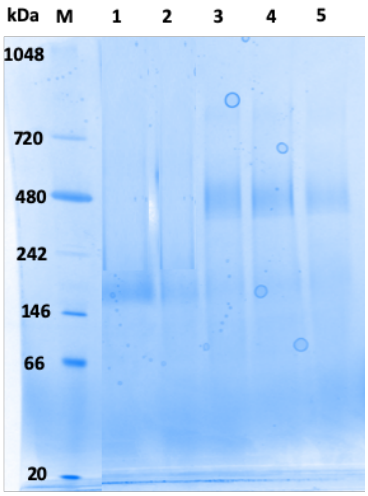

Figure 3.1I: Native gel of crosslinked components from *E. coli*. Lane 1 shows a non-crosslinked AccA3-D5-E5 sample. Lanes 2-5 show crosslinker added to the sample at 0.01, 0.02, 0.05 and 0.1% respectively.

The native gel shows crosslinked complexes electrophoresing at bands of approximately 400-480 kDa, perhaps suggesting smaller complexes than the originally predicted 750kDa dodecamer. Samples clearly showing strong crosslinking were taken for negative EM staining. This includes samples with 0.02%, 0.05% and 0.1% GA addition. Addition of 0.01% GA did not crosslink sufficiently as shown in lane 2 with complexes remaining at a similar size to without GA addition.

Negative Stain TEM images of E. coli AccA3-AccD5-AccE5

Investigation into ACCase complex formation was conducted using negative stain electron microscopy of the gel filtration samples (from figure 3.1H). Four images are shown in figure 3.1J. Image A has no crosslinker added, with B, C and D containing crosslinker glutaraldehyde (GA) at increasing concentrations. Protein concentrations of 0.05-0.08 mg/ml were optimal for imaging purposes. Visual analysis shows conformational heterogeneity of all samples, most likely with

degradation and low stability. However, crosslinker addition appears to make particles less crowded with improved resolution, especially at 0.1% GA addition in image D when compared to image A that is crowded, most likely containing contaminant particles. Particle sizes hypothesized to be protein complexes, as in image D, are approximately 10-15 nm.

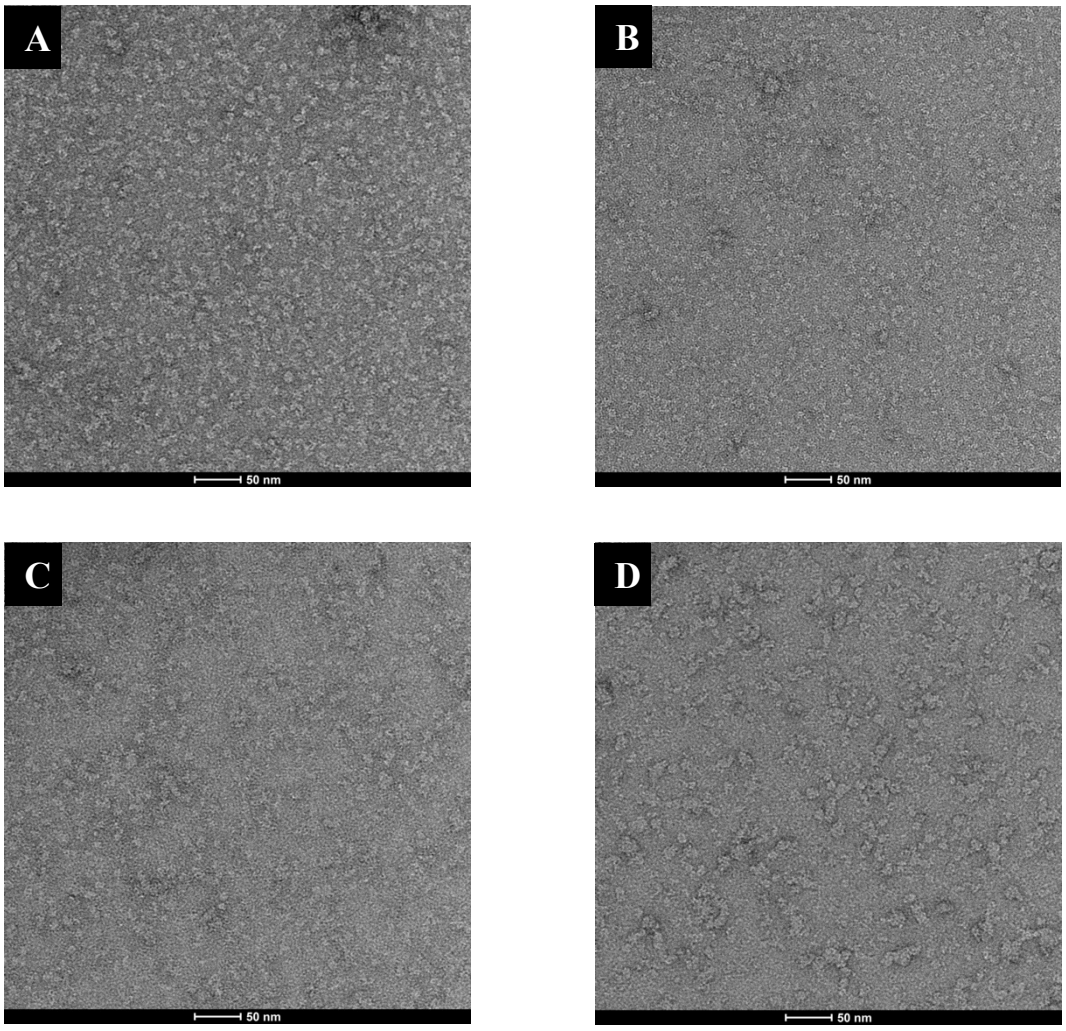

Figure 3.1J: Negative stain electron microscopy. Image A shows no crosslinker added. Images B, C and D show 0.02%, 0.05% and 0.1% GA addition, respectively.

3.2 Protein Purification and Imaging of M. smegmatis ACCase

Expression and Purification of M. smegmatis AccA3-AccD5-AccE5

After successful transformation of two plasmids co-expressed into g*roEL1ΔC* strains of *M. smegmatis*, one plasmid with AccA3 and another with AccD5-AccE5, (refer to methods for constructs), protein overexpression was induced and cells were harvested after incubation. An affinity chromatography run allowed isolation of the proteins within the complex from the supernatant of centrifuged mixtures, yielding ~25 mL of protein-containing fractions at concentrations of ~2 mg/mL . The affinity chromatogram and SDS PAGE gel are shown below in figures 3.2A and 3.2B, respectively.

Affinity Chromatography

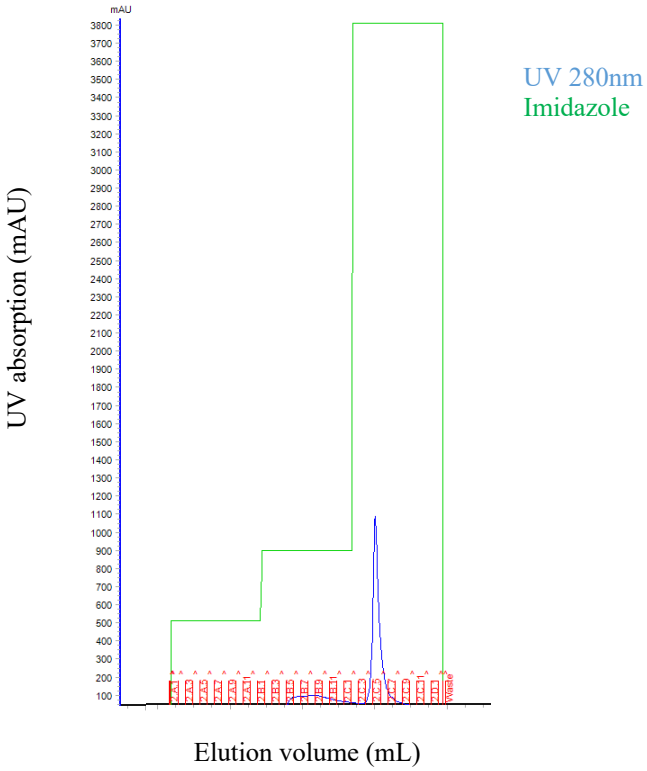

Figure 3.2A: Affinity chromatogram of AccA3-D5-E5. Imidazole addition is shown in green on the chromatogram with stepwise and linear additions shown. His-tagged protein is eluted into fractions 2B5-2C9.

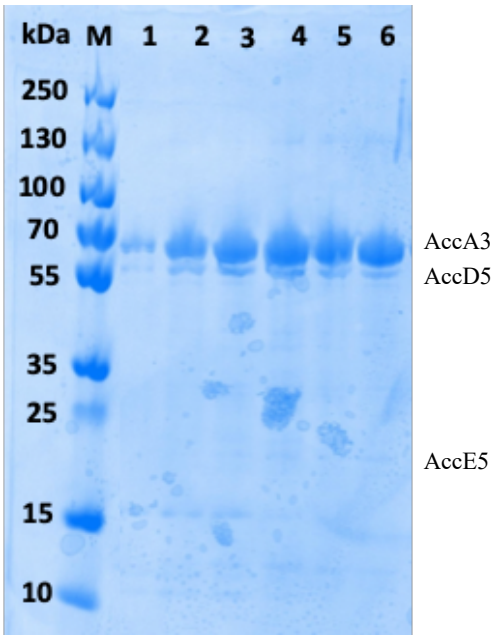

Figure 3.2B: SDS-PAGE gel of AccA3-D5-E5 HisTrap. Lanes 1-6 show AccA3 (64kDa) and AccD5 (59kDa) with low level expression of AccE5 (19kDa) in some of the lanes.

Figure 3.2A plots the elution volume (ml) against the UV absorption (mAU) of the eluted samples. As before with *E. coli*, stepwise and linear additions of imidazole were used. Fractions where our His-tagged protein elutes can be used for an SDS PAGE gel as in figure 3.2B. Gels show the sizes of AccA3 and AccD5 are approximately 64kDa and 59kDa respectively, as compared to the marker in lane M. Further observed were marked differences in expression between all three subunits, with low level expression of AccE5 at 19kDa near the base of the gel.

Crosslinking and Imaging of M. smegmatis AccA3-AccD5-AccE5

Crosslinking M. smegmatis ACCase components

Different to the procedure in *E. coli*, the plasmids in *M. smegmatis* cells have all 3 subunits co-expressed, meaning individual purifications were not required. Similar to the procedure with *E. coli*, subunits were crosslinked, with the SDS PAGE gel in figure 3.2C demonstrating greater complex formation (higher kDa bands) with crosslink addition, meaning individual subunit bands become less visible as they are presumably complexed. As an example, the size exclusion profile with 0.1% GA added is shown in figure 3.2D.

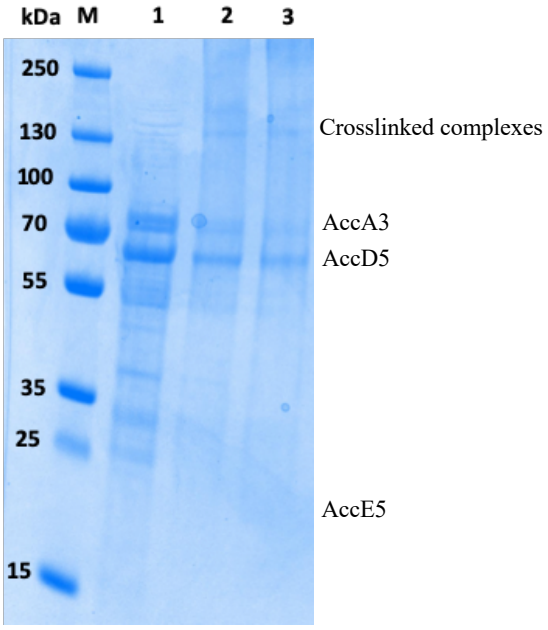

Figure 3.2C: SDS-PAGE gel of crosslinked AccA3-D5-E5 components from *M. smegmatis*. Lane 1 shows a non-crosslinked AccA3-D5-E5 sample. Lanes 2 and 3 show crosslinker added to the sample at 0.05% and 0.1% respectively.

Size Exclusion Chromatography

Crosslinked samples from the HisTrap study were optimised for SEC to a concentration of 0.05 mg/mL. Figures 3.2D and 3.2E show the SEC elution profile with UV_{280nm} absorption and the native gel from SEC samples, respectively. Non-crosslinked samples are approximately 140kDa and crosslinked samples are nearer to 350kDa.

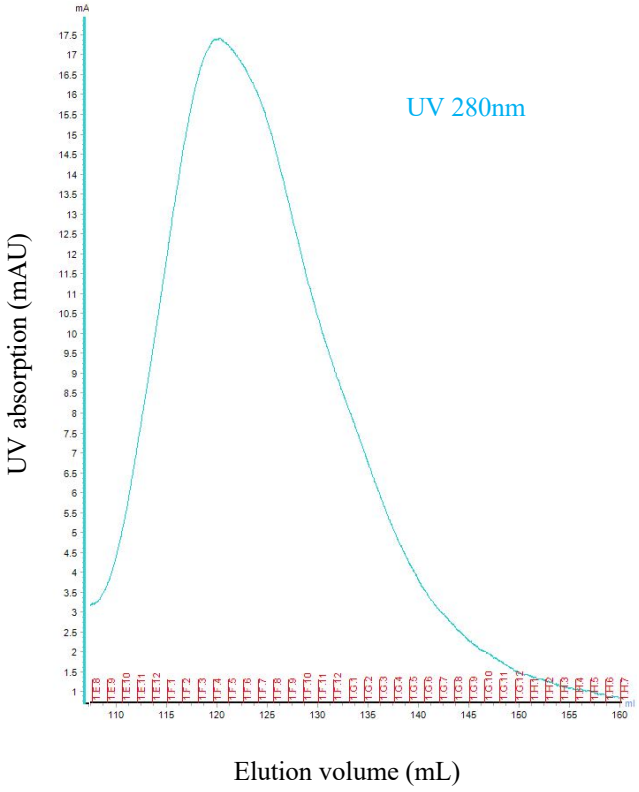

Figure 3.2D: Size exclusion profile of AccA3-D5-E5 complex with elution into fractions 1E8-1H7.

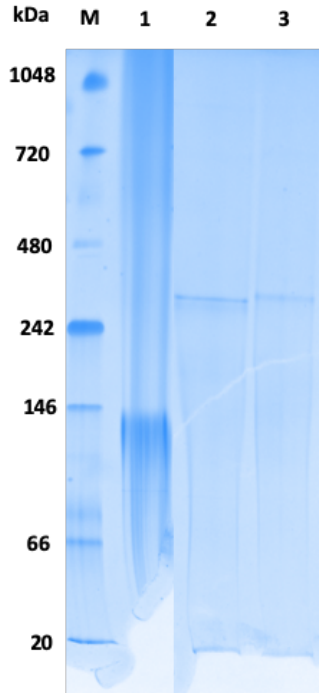

Figure 3.2E: Native gel of crosslinked AccA3-D5-E5 components from *M. smegmatis*. Lane 1 shows a non-crosslinked AccA3-D5-E5 sample. Lanes 2 and 3 show crosslinker added to the sample at 0.05% and 0.1% respectively.

Samples containing 0.05% and 0.1% GA crosslinker demonstrate strong crosslinking in the native gel. As before with *E. coli*, the same samples from the gel filtration were taken forward for imaging.

Negative Stain TEM images of M. smegmatis AccA3-AccD5-AccE5

As before with *E. coli*, imaging of *M. smegmatis* complexes was conducted using negative stain electron microscopy. Shown in figure 3.2F are micrographs of ACCase complexes. Image A has no crosslinker added. Image B has 0.05% GA added. Images C and D have 0.1% GA added. Protein concentrations of 0.05-0.08 mg/ml were optimal for imaging purposes. Visual analysis again shows conformational heterogeneity of all samples, with images crosslinked protein being less crowded. Particle sizes are approximately 10-15 nm. Images C and D show complexes that appear to form pentameric or hexameric ring formations as annotated by the magnified perspective. Ring formations have an approximate 10nm diameter. These could be artefacts of our experiment and are discussed later.

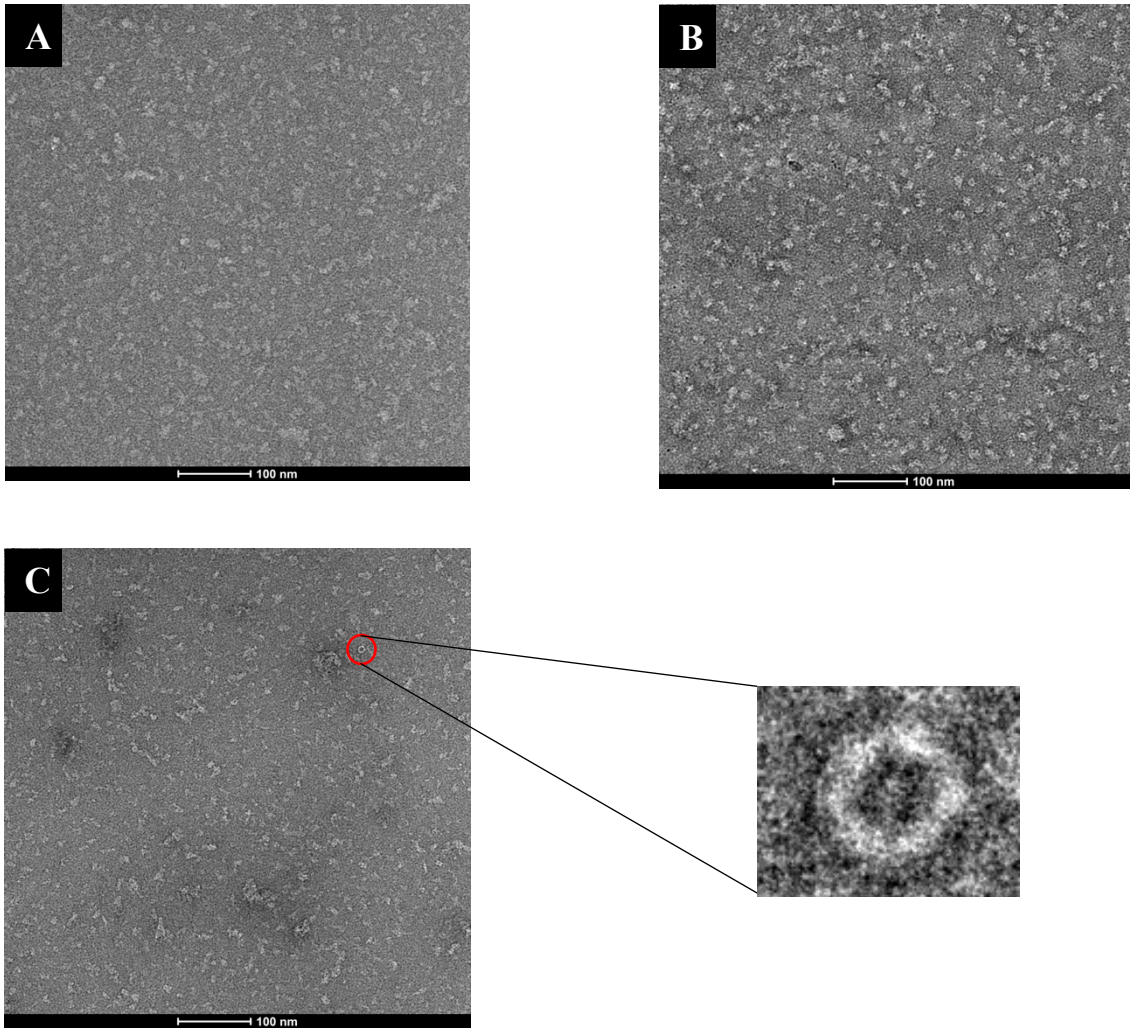

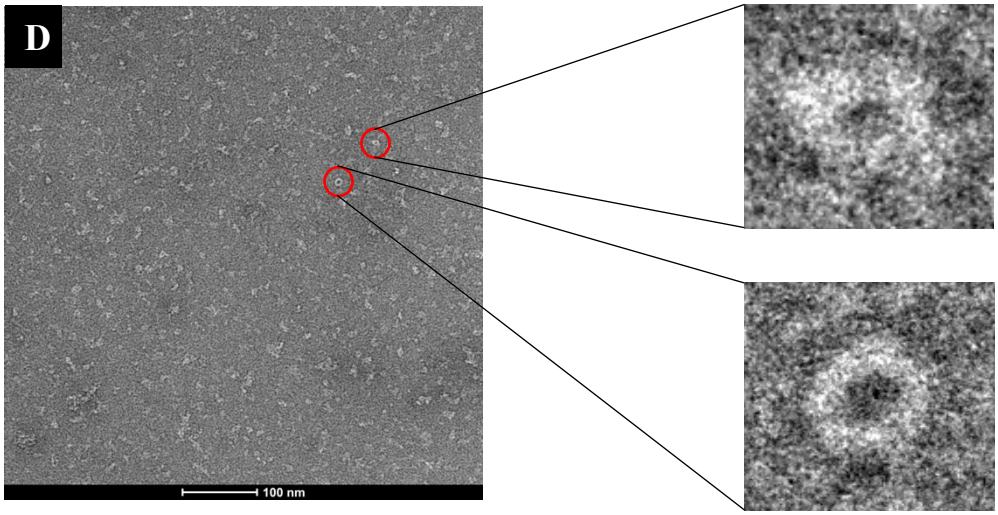

Figure 3.2F: Negative stain electron microscopy. Image A shows no crosslinker added. Images B, C and D show 0.05%, 0.1% and 0.1% GA addition, respectively, with magnified complexes from C and D displayed.

3.3 Kinetic characterisation of ACCase complexes from M. smegmatis

Kinetic assay data of M. smegmatis AccA3-AccD5-AccE5

The AccA3-AccD5-AccE5 complex isolated and crosslinked from *M. smegmatis* bacteria was utilized *in vitro* to demonstrate catalytic activity. Figure 3.3 shows the complex is active *in vitro* and is based on a spectrophotometric assay measuring NADH oxidation at 340nm (see methods for reaction details). The change in absorbance of NADH can be measured over 3 repetitions (5 min reaction time) to calculate the rate of reaction with increasing substrate addition. The final concentration of the enzyme complex used was 0.35 mg/ml. This allowed determination of Michaelis-Menten parameters for the carboxylase activity using the Beer-Lambert Law: V_{max} = 1.22 mM min^{-1} mg^{-1} and K_M = 0.86 mM. The raw data set and concentrations of each component are shown in the appendix.

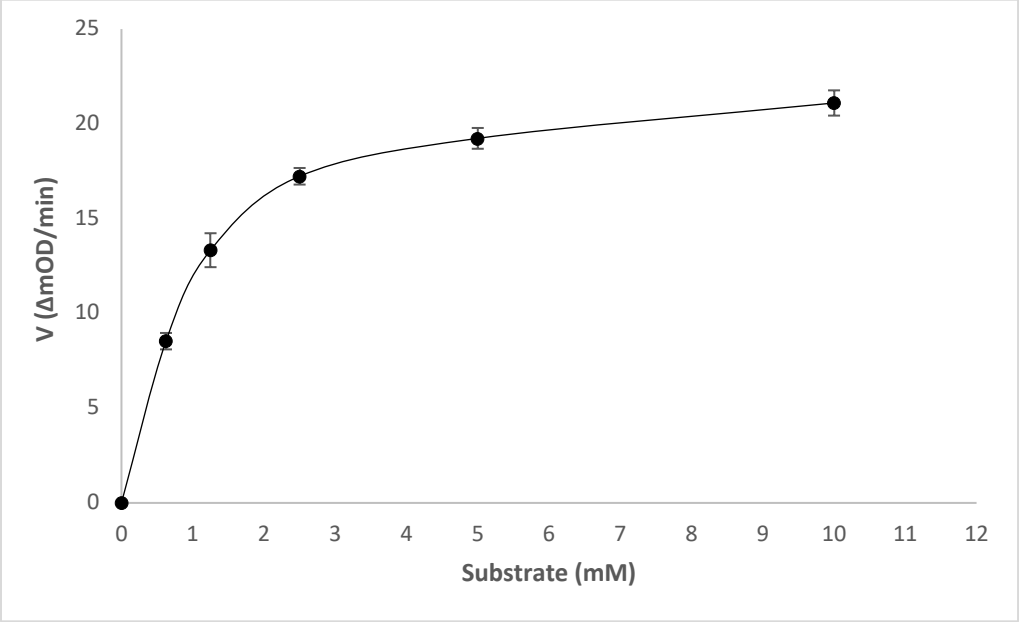

Figure 3.3: AccA3-AccD5-AccE5 *in vitro* shows catalytic activity when using Acetyl CoA as a substrate. The mean rate of reaction is plotted against increasing substrate concentration using non-linear regression analysis in Microsoft Excel. Error bars are derived from three repetitions.

4. Discussion

In the present study, AccA3-AccD5-AccE5 complexes from *E. coli* and *M. smegmatis* involved in the committed step of mycolic acid biosynthesis were successfully overexpressed and purified using a combination of affinity and size exclusion chromatography. Complexes were then subjected to imaging and kinetic analyses. However, limitations were identified at the purification and imaging stages of our approach.

Protein expression and purification

Previous research shows evidence for approximately 750 kDa dodecameric AccA1-AccD1 and AccA2-AccD2 complexes, with these α and β subunits forming a series of trimeric or hexameric complexes of a 1:1 stoichiometry (Huang *et al*., 2011). Our study shows with both species of bacteria, the molecular weights of the AccA3/AccD5 subunits purified appear consistent with previous research. However, an inconsistency is the overall molecular weight of the complexes formed. Initially, this study was attempted using no crosslinking reagent, with complexes of 140-180 kDa forming, as shown on native PAGE gels. Addition of crosslinker assisted complex formation, with complexes of 400-480 kDa now forming, still falling short of the previously identified 750 kDa related complexes. To generate improved complex stability, the optimal crosslinker concentration was 0.02-0.1% glutaraldehyde. Our observed molecular weight of 400-480 kDa would suggest smaller complex formations, such as hexamers or octamers, if indeed complexes are forming. The use of crosslinking reagents was partly effective here, as with previous studies (Bala et *al*., 2014, Slusarewicz *et al*., 2010).

An initial observation of note was the differences in expression levels of the individual subunits shown on electrophoresis gels in our study, especially the low levels of AccE5, a monomer proposed to improve complex stability and substrate access to enzyme active sites (Oh *et al*., 2006, Gago *et al*., 2006). Despite the predicted 1:1 stoichiometry between α and β subunits, a mismatch in protein subunit concentration is not uncommon as one subunit may display functions elsewhere or could be regulated by different transcription factors, as show in Figure 3.2B with a lack of

stoichiometry between AccA3 and AccD5 - the reasons for which are still speculative. Lack of expression coherence due to multi-functionality or differences in transcriptional regulation have been demonstrated in *E. coli* and *Saccharomyces cerevisiae* (Leake *et al*., 2006, Gavin *et al*., 2006). With regards to AccE5, a previous study also had issues generating a concentrated and stable solution of AccE5 (Anandhakrishnan, 2013). This was proposed to be a result of a lack of secondary structure formation *in vitro*, as verified by circular dichroism (CD) spectroscopy (Anandhakrishnan, 2013). This could mean once purified alongside AccA3 and AccD5, AccE5 unfolds and so the full complex is no longer stabilised. Perhaps the lower AccE5 stability was partly accounted for by the addition of a crosslinker. Furthermore, both SDS and native PAGE gels show contamination from other endogenous proteins or perhaps degraded protein complexes. Contamination of AccE5 samples may have also contributed to the larger than predicted AccE5 molecular weight, leading to a subsequent effect on complex formation and stability. The heterogeneity of our sample is almost certainly contributing to lower stability of our full complex (Wingfield, 2015). Methods to reduce protein contamination are discussed later.

Negative stain electron microscopy

Negative stain electron microscopy showed similar complex particle sizes to previous studies (Ehebauer *et al*., 2015). Crosslinking samples certainly improved complex formation and homogeneity, thereby reducing particle crowding. This was most apparent at 0.05% and 0.1% glutaraldehyde addition, which may be high enough for intermolecular crosslinks, but not too high that intramolecular crosslinks become an issue (Oveimar *et al*., 2014). However, also shown was monomeric protein and most likely contamination of the sample. Stability is an issue and is visible with both *E. coli* and *M. smegmatis* complexes. Discussed here are the imaging observations and how we can reduce contamination and improve stability of our sample in the future.

An interesting observation in *M. smegmatis* samples were ring-like complexes. This is potentially new information of how the complex can form, rather than the previously identified dodecameric form of AccA1-AccD1 and AccA2-AccD2 (Ehebauer *et al*., 2015). When comparing EM images to the native gel, we could conclude there exists a hexameric or octameric complex based on molecular weights. However, given the low or potentially absent AccE5 expression, the ring-like

complexes we observe may simply be oligomers of AccA3 or AccD5 on their own or bound together that are unable to form a stable dodecamer, or indeed artefacts of our experiment. Hexameric formations of AccA3-AccD5 crystals have been previously studied and this may be what we are observing (Ting-Wan *et al*., 2006). This could be confirmed with peptide mass fingerprinting to identify both the composition of the hexameric complexes, as well as the nature of the contaminant proteins co-eluting with our target protein that may be responsible for the ring-like formations (Tiengo *et al*, 2009).

Protein purity and stability

There are a number of means that could be utilized to improve protein purity or stability. To improve protein purity, attempts to reduce endogenous protein contamination could involve repeating the already established purification steps, or use a range of purification techniques. Other purification techniques we could apply to our sample could be anion exchange, hydrophobic interaction or hydroxyapatite chromatography. When combined prior to size exclusion chromatography, this can help reduce host cell contaminant protein, aggregates, endotoxins and DNA from recombinant proteins (Larry *et al*., 2009). This would also contribute to improving complex formation and stability (Wang *et al*., 2014).

Other ways to improve complex stability would be via using a greater range of crosslinking variables, increasing AccE5 expression levels or introducing a substrate. Our crosslinking studies were helpful for initial studies into improving complex formation of our ACCase enzyme. Further studies should utilise a greater range of glutaraldehyde concentrations, different durations exposed to the crosslinker and perhaps try different intermolecular crosslinking reagents such as dimethyl adipimidate (DMA) or dimethyl suberimidate (DMS) (Zhenzhan *et al*., 2004). This may help optimise the crosslinking procedure and maximise the chance of achieving complex stability with this technique. Literature on similar studies indicate the need for AccE5 to aid stability of AccA3 and AccD5 when forming a dodecameric complex together (Oh *et al*., 2006). We could take expressed and purified AccE5 protein and exogenously add this to co-expressed AccA3-AccD5. This may be necessary because as seen in gels, AccE5 expression is low or potentially absent. Using separately expressed AccE5 for *M. smegmatis* may be necessary in order to ensure sufficient

AccE5 is available to aid complex stability. Any improvements to stability could be screened for using either Differential Scanning Calorimetry (DSC) or Thermal Shift Assays (TSA) (Bruce *et al*., 2019).

The introduction of proposed enzyme substrates could help with enzyme stability (Wurth *et al*., 2001). A study by Wurth *et al* shows addition of substrates can modify enzyme conformation to increase levels of order and stability, as measured by thermal denaturation experiments and far-UV circular dichroism (CD). This could be applied to our study with addition of known substrates of ACCase such as saturated organic acids acetyl CoA and propionyl CoA or unsaturated counterparts 3-methylcrotonyl-CoA and geranyl-CoA. Increasing enzyme stability may improve complex formation for EM images and further studies.

Kinetic assay of M. smegmatis ACCase

Kinetic data collected using a well-established enzyme-coupled assay shows our purified complex is active *in vitro*. This assay did not work in *E. coli*. This may be explained by using the near-native host *M. smegmatis* that ensures proper protein folding and processing, generating sufficient catalytic activity *in vitro*.

In a previous study, a V_{max} of 1.33 mM min^{-1} mg^{-1} was generated for the same complex as ours (Gago *et al*., 2006). Our calculated V_{max} of 1.22 mM min^{-1} mg^{-1} is comparable to this study. A possible explanation for higher maximal activity in the previous study is they used a ratio of AccE5 to AccA3-AccD5 of 5:1 compared to our 1:1, perhaps improving complex stability and thus boosting maximal catalytic activity. However, this research group were also challenged with EM imaging (and crystallisation) of the complex, despite increasing the ratio of the AccE5 subunit.

This may suggest that expression levels of AccE5 are not too important for protein stability and thus catalytic activity. Perhaps substrate presence is more important, given that our study and others have varying AccE5 expression levels, yet similar kinetic outputs and problems with imaging. This reinforces the idea that substrate addition prior to imaging may improve complex stability. An additional outcome from this kinetic assay is that the previously proposed

dodecameric structure may not be needed for an active enzyme, at least *in vitro*. Our data produced some full complexes, but with the majority not in a complete complex, yet our enzyme demonstrated catalytic activity. In a previous study AccA3 and AccD5 were shown to demonstrate activity as (hetero)hexamers - perhaps this is what we have observed (Lin *et al*., 2006).

This may have wider implications when using TB metabolism as a drug target. Lipid biosynthetic enzymes may not need a full complex to form but can function as separate subunits. Therefore, perhaps the focus of drug targeting should look at not only preventing complex formation, but also investigate structural inhibition of AccA3-AccD5 oligomers, thereby reducing substrate access.

Conclusion

The present study has interesting implications for the research into mycobacterial metabolic enzymes. Our study, like previous studies, has shown there are difficulties in maintaining a stable and pure protein complex of enzymes involved in mycolic acid biosynthesis. However, we can provide speculative results of an active enzyme *in vitro*, either in dodecameric form or hexameric AccA3-AccD5. This is based on complex molecular weight knowledge obtained from previous studies and what is observed in this study.

If the suggestions of increasing AccE5 expression combined with the addition of a substrate were taken in further studies, perhaps improved complex formation would be observed. This could improve the chances of achieving cryo-EM structures or encourage attempts at crystallising the complex to attain diffraction patterns. We have opened a new avenue by providing kinetic data with this complex that may not be in dodecameric form. This could mean that for studying metabolic enzymes in TB, valuable structures are also found in the subunit alone as these appear to maintain activity. Therefore, the subunits themselves could still be considered useful potential drug targets and if inhibited may slow TB infections. If subunits do function alone, preventing substrate access to subunits or using competitive analogs may be a more viable therapy than preventing complex formation. This approach has been shown before in a study and review that showed substrate access and inhibition are potent means to inhibit TB growth (Hassan *et al*., 2018, Duckworth *et al*., 2012).

5. Future Perspectives

The objective of the study was to optimise the process of obtaining purified ACCase enzyme complexes involved in the committed step of mycobacterial mycolic acid biosynthesis. Further to this, explore the capability of using negative stain EM and kinetic assays to understand if complexes formed were suitable for crystallisation trials and showed catalytic activity. Elucidating the structure and activity of such complexes could be fundamental to future experimental approaches and downstream structural drug design.

Our study did not obtain a homogeneous solution of dodecameric complexes formed, as hoped for based on previous experimental data. The reasons for this have been discussed. I propose future studies utilise the addition of substrates or substrate analogs, extra crosslinking variables or further increasing AccE5 expression in order to improve the chances of achieving the proposed dodecameric complex. If larger complexes are formed near to 750 kDa, then perhaps performing more advanced imaging studies becomes more viable.

Interestingly, the study shows that the expressed protein is forming particles of heterogeneous size, some similar to the size of the dodecameric complex (750 kDa), with others appearing hexameric according to molecular weight. This has highlighted the possibility that expressed protein complexes that may be AccA3 or AccD5 alone, could function independently due to the catalytic activity observed. Separate kinetic assays using AccA3 or AccD5 alone could be complementary to further providing evidence for this. In addition, this could demonstrate that one of the components is contributing more than the other to the perceived activity observed in this study.

With regards to the impact of our study on drug design in this field of TB treatment, this could change the perspective of how to design such therapies. Perhaps if the enzyme can function as a smaller complex, the focus should perhaps be on reducing substrate access or inhibiting AccA3-AccD5 hexamers rather than inhibiting dodecameric complex formation. Overcoming the hurdles faced in this study would be essential for furthering research in this direction.

REFERENCES

Abrahams, K. A., & Besra, G. S. (2018). Mycobacterial cell wall biosynthesis: a multifaceted antibiotic target. *Parasitology*, 145(2), 116–133.

Adamis G, Papaioannou MG, Giamarellos-Bourboulis EJ, Gargalianos P, Kosmidis J & Giamarellou H (2004) Pharmacokinetic interactions of ceftazidime, imipenem and aztreonam with amikacin in healthy volunteers. *Int J Antimicrob Agents* 23: 144-149.

Ames GF (1974). Resolution of bacterial proteins by polyacrylamide gel electrophoresis on slabs. Membrane, soluble, and periplasmic fractions. *J Biol Chem*. 249(2):634-44.

Anandhakrishnan. M (2013) Structural and Functional Studies on Acyl-CoA Carboxylases of *Mycobacterium Tuberculosis*. Ph.D thesis. *University of Heidelberg, Germany.*

Andries K, Verhasselt P, Guillemont J, et al. (2005) A diarylquinoline drug active on the ATP synthase of Mycobacterium tuberculosis. *Science* 307: 223-227.

Angala SK, Belardinelli JM, Huc-Claustre E, Wheat WH and Jackson M (2014) The cell envelope glycoconjugates of Mycobacterium tuberculosis. *Crit. Rev. Biochem. Mol. Biol* 49, 361–399

Bala S, Sharma N, Kajal A, Kamboj S, Saini V (2014) Mannich bases: an important pharmacophore in present scenario. *Int J Med Chem*. Volume 2014, Article ID 191072.

Balasubramanian V, Pavelka MS, Jr, Bardarov SS, Martin J, Weisbrod TR, McAdam RA, Bloom BR, Jacobs WR., Jr (1996) Allelic exchange in Mycobacterium tuberculosis with long linear recombination substrates. *J Bacteriol*. 178:273–279.

Bérdy, J (2005) Bioactive Microbial Metabolites. *J Antibiot* 58, 1–26.

Berg JM, Tymoczko JL, Stryer L (2002) Fatty Acids Are Synthesized and Degraded by Different Pathways. *Biochemistry, WH Freeman.* 5th edition.

Bhatt A, Kremer L, Dai AZ, Sacchettini JC & Jacobs WR, Jr. (2005) Conditional depletion of KasA, a key enzyme of mycolic acid biosynthesis, leads to mycobacterial cell lysis. *J Bacteriol* 187: 7596-7606.

Bhatt A, Molle V, Besra GS, Jacobs WR, Jr. & Kremer L (2007) The Mycobacterium tuberculosis FAS-II condensing enzymes: their role in mycolic acid biosynthesis, acid-fastness, pathogenesis and in future drug development. *Mol Microbiol* 64: 1442-1454.

Blanco S, Prat C, Pallarés MA, Matas L, Domínguez J (2004) Centrifugal ultrafiltration method for rapid concentration of Legionella pneumophila urinary antigen. *J Clin Microbiol.* 42(9):4410

Blumberg HM, Burman WJ, Chaisson RE, et al. (2003) American Thoracic Society/Centers for Disease Control and Prevention/Infectious Diseases Society of America: treatment of tuberculosis. *Am J Respir Crit Care Med* 167: 603-662.

Bogner. A, P.H. Jouneau, G. Thollet, D. Basset, C. Gauthier (2007) A history of scanning electron microscopy developments: Towards ‘‘wet-STEM’’ imaging. *Micron.* 38 (2007) 390–401.

Bornhorst, J. A., & Falke, J. J. (2000). Purification of proteins using polyhistidine affinity tags. *Methods in enzymology*, 326, 245–254.

Brennan, P. J. and Nikaido, H. (1995). The envelope of mycobacteria. *Annual Review of Biochemistry*. 64, 29–63.

Briken V, Porcelli SA, Besra GS & Kremer L (2004) Mycobacterial lipoarabinomannan and related lipoglycans: from biogenesis to modulation of the immune response. *Mol Microbiol* 53: 391-403.

Brown AK, Bhatt A, Singh A, Saparia E, Evans AF & Besra GS (2007) Identification of the dehydratase component of the mycobacterial mycolic acid-synthesizing fatty acid synthase-II complex. *Microbiology* 153: 4166-4173.

Bruce, D., Cardew, E., Freitag-Pohl, S., Pohl, E. (2009) How to Stabilize Protein: Stability Screens for Thermal Shift Assays and Nano Differential Scanning Fluorimetry in the Virus-X Project. *J. Vis. Exp.* (144), e58666.

Burman WJ, Gallicano K & Peloquin C (2001) Comparative pharmacokinetics and pharmacodynamics of the rifamycin antibacterials. *Clin Pharmacokinet* 40: 327-341.

Camus JC, Pryor MJ, Medigue C & Cole ST (2002) Re-annotation of the genome sequence of Mycobacterium tuberculosis H37Rv. *Microbiology* 148: 2967-2973.

Cole ST, Brosch R, Parkhill J, et al. (1998) Deciphering the biology of Mycobacterium tuberculosis from the complete genome sequence. *Nature* 393: 537-544.

Costas M. (1995) The Analysis of Bacterial Proteins by SDS Polyacrylamide Gel Electrophoresis.. *Humana Press*. In: Howard J., Whitcombe D.M. (eds) Diagnostic Bacteriology Protocols: Methods in Molecular Biology, vol 46.

Crowle AJ, Dahl R, Ross E & May MH (1991) Evidence that vesicles containing living, virulent Mycobacterium tuberculosis or Mycobacterium avium in cultured human macrophages are not acidic. *Infect Immun* 59: 1823-1831.

Cynamon M, Sklaney MR & Shoen C (2007) Gatifloxacin in combination with rifampicin in a murine tuberculosis model. *J Antimicrob Chemother* 60: 429-432.

Cywes C, Hoppe HC, Daffe M and Ehlers MR (1997) Nonopsonic binding of Mycobacterium tuberculosis to complement receptor type 3 is mediated by capsular polysaccharides and is strain dependent. *Infect. Immun* 65, 4258–4266

Dalton T, Cegielski P, Akksilp S, et al. (2012) Prevalence of and risk factors for resistance to second-line drugs in people with multidrug-resistant tuberculosis in eight countries: a prospective cohort study. *Lancet* 380: 1406-1417.

Dannenberg AM, Jr. (1994) Roles of cytotoxic delayed-type hypersensitivity and macrophage-activating cell-mediated immunity in the pathogenesis of tuberculosis. *Immunobiology* 191: 461-473.

David J. Lea-Smith, James S. Pyke, Dedreia Tull, Malcolm J. McConville, Ross L. Coppel, and Paul K. Crellin (2007) The Reductase That Catalyzes Mycolic Motif Synthesis IsRequired for Efficient Attachment of Mycolic Acidsto Arabinogalactan. *The Journal of Biological Chemistry*.Vol 282 (15), pp. 11000–11008.

De Haan, K., Ballard, Z. S., Rivenson, Y., Wu, Y., & Ozcan, A. (2019). Resolution enhancement in scanning electron microscopy using deep learning. *Scientific reports*, 9(1), 12050.

Dhakal D, Pokhrel AR, Shrestha B and Sohng JK (2017) Marine Rare Actinobacteria: Isolation, Characterization, and Strategies for Harnessing Bioactive Compounds. *Front. Microbiol.* 8:1106.

Diacovich L, Peiru S, Kurth D, Rodriguez E, Podesta F, Khosla C & Gramajo H (2002) Kinetic and Structural Analysis of a New Group of Acyl-CoA Carboxylases Found in Streptomyces coelicolor A3(2). *Journal of Biological Chemistry* 277: 31228-31236.

Diana Mikiewicz, Andrzej Plucienniczak, Anna Bierczynska-Krzysik, Agnieszka Skowronek, Grzegorz Wegrzyn (2019) Novel Expression Vectors Based on the pIGDM1 Plasmid. *Molecular Biotechnology*. Volume 61, Issue 10, pp 763–77.

Draper P., Khoo K. H., Chatterjee D., Dell A. and Morris H. R. (1997). Galactosamine in walls of slow-growing mycobacteria. *Biochemical Journal 327* (Pt 2), 519–525.

Duckworth, B. P., Nelson, K. M., & Aldrich, C. C. (2012). Adenylating enzymes in Mycobacterium tuberculosis as drug targets. *Current topics in medicinal chemistry*, 12(7), 766–796.

Dwyer, D.J., M.A. Kohanski & J.J. Collins (2009) Role of reactive oxygen species in antibiotic action and resistance. *Curr. Opin. Microbiol*. 12: 482–489.

Ehebauer MT & Wilmanns M (2011) The progress made in determining the Mycobacterium tuberculosis structural proteome. *Proteomics* 11: 3128-3133.

Ehebauer, M. T., Zimmermann, M., Jakobi, A. J., Noens, E. E., Laubitz, D., Cichocki, B., … Wilmanns, M. (2015). Characterization of the mycobacterial acyl-CoA carboxylase holo complexes reveals their functional expansion into amino acid catabolism. *PLoS pathogens,* 11(2), e1004623.

Fernandes ND, Kolattukudy PE (1996) Cloning, sequencing and characterization of a fatty acid synthase-encoding gene from Mycobacterium tuberculosis var. bovis BCG. *Gene*. 170: 95-99.

Flynn JL & Chan J (2005) What's good for the host is good for the bug. *Trends Microbiol 13: 98-102.*

Forster-Fromme K, Jendrossek D. (2010) Catabolism of citronellol and related acyclic terpenoids in pseudomonads. *Appl Microbiol Biotechnol*. 87:859–869.

Fox HH (1952) The chemical approach to the control of tuberculosis. *Science*. 116(3006):129-34.

Frehel C, de Chastellier C, Lang T & Rastogi N (1986) Evidence for inhibition of fusion of lysosomal and prelysosomal compartments with phagosomes in macrophages infected with pathogenic Mycobacterium avium. *Infect Immun* 52: 252-262.

Gago G, Diacovich L, Arabolaza A, Tsai SC, Gramajo H. (2011) Fatty acid biosynthesis in actinomycetes. *FEMS Microbiol Rev*. 35:475–49.

Gago G, Kurth D, Diacovich L, Tsai SC & Gramajo H (2006) Biochemical and structural characterization of an essential acyl coenzyme A carboxylase from Mycobacterium tuberculosis. *J Bacteriol* 188: 477-486.

Gallagher, J. R., Kim, A. J., Gulati, N. M., & Harris, A. K. (2019). Negative-stain transmission electron microscopy of molecular complexes for image analysis by 2D class averaging. *Current Protocols in Microbiology*, 54, e90.

Gande R, Dover LG, Krumbach K, Besra GS, Sahm H, Oikawa T & Eggeling L (2007) The Two Carboxylases of Corynebacterium glutamicum Essential for Fatty Acid and Mycolic Acid Synthesis. *Journal of Bacteriology* 189: 5257-5264.

Gavalda S, Bardou F, Laval F, Bon C, Malaga W, Chalut C, Guilhot C, Mourey L, Daffé M, Quémard A (2014) The polyketide synthase Pks13 catalyzes a novel mechanism of lipid transfer in mycobacteria. *Chem Biol*. 18;21(12):1660-9.

Gavin A.C, P. Aloy, P. Grandi, R. Krause, M. Boesche, M. Marzioch, C. Rau, L.J. Jensen, S. Bastuck, B. Dümpelfeld, et al. (2006) Proteome survey reveals modularity of the yeast cell machinery. *Nature*, 440, pp. 631-636.

Glickman MS, Cox JS & Jacobs WR, Jr. (2000) A novel mycolic acid cyclopropane synthetase is required for cording, persistence, and virulence of Mycobacterium tuberculosis. *Mol Cell* 5: 717-727.

Goren MB (1972) Mycobacterial lipids: selected topics. *Bacteriol Rev* 36: 33-64.

Goude R, Parish T (2009) Electroporation of mycobacteria. *Methods Mol Biol*. 465: 203-15.

Griffin JE, Gawronski JD, Dejesus MA, Ioerger TR, Akerley BJ & Sassetti CM (2011) Highresolution phenotypic profiling defines genes essential for mycobacterial growth and cholesterol catabolism. *PLoS Pathog* 7: e1002251.

Guerardel Y, Maes E, Elass E, et al. (2002) Structural study of lipomannan and lipoarabinomannan from Mycobacterium chelonae. Presence of unusual components with alpha 1,3-mannopyranose side chains. *J Biol Chem* 277: 30635-30648.

Gurumurthy, M., M. Rao, T. Mukherjee, et al. (2013). A novel F(420) -dependent anti-oxidant mechanism protects Mycobacterium tuberculosis against oxidative stress and bactericidal agents. *Mol. Microbiol.* 87: 744–755.

Harrison J., Lloyd G., Joe M., Lowary T. L., Reynolds E., Walters-Morgan H., Bhatt A., Lovering A., Besra G. S. and Alderwick L. J. (2016). *American Society for Microbiology* 7, e00972.

Harwood JL (1998) Fatty acid metabolism. *Annu Rev Plant Physiol Plant Mol Biol*, 39: 101-138.

Hassan, S., Šudomová, M., Berchová-Bímová, K., Gowrishankar, S., & Rengasamy, K. (2018). Antimycobacterial, Enzyme Inhibition, and Molecular Interaction Studies of Psoromic Acid in Mycobacterium tuberculosis: Efficacy and Safety Investigations. *Journal of clinical medicine,* 7(8), 226.

Holton SJ, King-Scott S, Eddine AN, Kaufmann SHE & Wilmanns M (2006) Structural diversity in the six-fold redundant set of acyl-CoA carboxyltransferases in Mycobacterium tuberculosis. *FEBS Letters* 580: 6898-6902.

Huang CS, Ge P, Zhou ZH & Tong L (2011) An unanticipated architecture of the 750-kDa "6!6 holoenzyme of 3-methylcrotonyl-CoA carboxylase. *Nature* 481: 219-223.

Hunter RL, Olsen MR, Jagannath C & Actor JK (2006) Multiple roles of cord factor in the pathogenesis of primary, secondary, and cavitary tuberculosis, including a revised description of the pathology of secondary disease. *Ann Clin Lab Sci* 36: 371-386.

Inoue H, Nojima H & Okayama H (1990) High efficiency transformation of Escherichia coli with plasmids. *Gene* 96: 23-28.

Ishizaki Y., Hayashi C., Inoue K., Igarashi M., Takahashi Y., Pujari V., Crick D. C., Brennan P. J. and Nomoto A. (2013). Inhibition of the first step in synthesis of the mycobacterial cell wall core, catalyzed by the GlcNAc-1-phosphate transferase WecA, by the novel caprazamycin derivative CPZEN-45. *Journal of Biological Chemistry* 288, 30309–30319.

Jia L, Tomaszewski JE, Hanrahan C, et al. (2005) Pharmacodynamics and pharmacokinetics of SQ109, a new diamine-based antitubercular drug. *Br J Pharmacol* 144: 80-87.

Jeong, H., Kim, H. J., & Lee, S. J. (2015). Complete Genome Sequence of Escherichia coli Strain BL21. *Genome announcements*, 3(2).

Kaplan G, Post FA, Moreira AL, et al. (2003) Mycobacterium tuberculosis growth at the cavity surface: a microenvironment with failed immunity. *Infect Immun* 71: 7099-7108.

Kartheek Gavini, Kodeeswaran Parameshwaran (2019) Western Blot (Protein Immunoblot). *StatPearls Publishing*. Bookshelf ID: NBK542290PMID: 31194430.

Kauffmann, S.H.E. (2004). New issues in tuberculosis. *Ann. Rheum. Dis*. 63: 1150–1156.

Khasnobis S, Escuyer VE & Chatterjee D (2002) Emerging therapeutic targets in tuberculosis: post-genomic era. *Expert Opin Ther Targets* 6: 21-40.

Kostylev, M., Otwell, A. E., Richardson, R. E., & Suzuki, Y. (2015). Cloning Should Be Simple: Escherichia coli DH5α-Mediated Assembly of Multiple DNA Fragments with Short End Homologies. *PloS one*, 10(9).

Knowles JR (1989) The mechanism of biotin-dependent enzymes. *Ann Rev Biochem*. 58:195–221

Kurth DG, Gago GM, de la Iglesia A, et al. (2009) ACCase 6 is the essential acetyl-CoA carboxylase involved in fatty acid and mycolic acid biosynthesis in mycobacteria. *Microbiology* 155: 2664-2675.

La Verde, V., Dominici, P. and Astegno, A. (2017). Determination of Hydrodynamic Radius of Proteins by Size Exclusion Chromatography. *Bio-protocol* 7(8).

Larry J. Cummings, Mark A. Snyder, Kimberly Brisack (2009) Chapter 24 Protein Chromatography on Hydroxyapatite Columns. *Methods in Enzymology*. Volume 463, Pages 387-404.

Leake M.C, J.H. Chandler, G.H. Wadhams, F.Bai, R.M. Berry, J.P. Armitage (2006) Stoichiometry and turnover in single, functioning membrane protein complexes. *Nature*, 443, pp. 355-358.

Lemassu A & Daffe M (1994) Structural features of the exocellular polysaccharides of Mycobacterium tuberculosis. *Biochem J* 297 (Pt 2): 351-357.

Liang, W., Xu, L., Sui, Z., Li, Y., Li, L., Wen, Y., Li, C., Ren, S., & Liu, G. (2016). Quantification of plasmid DNA reference materials for Shiga toxin-producing Escherichia coli based on UV, HR-ICP-MS and digital PCR. *Chemistry Central journal*, 10(1), 55.

Lienhardt C, Lönnroth K, Menzies D, Balasegaram M, Chakaya J, Cobelens F, et al. (2016) Translational Research for Tuberculosis Elimination: Priorities, Challenges, and Actions. PLoS Med 13(3): e1001965.

Lin, T. W., Melgar, M. M., Kurth, D., Swamidass, S. J., Purdon, J., Tseng, T., Gago, G., Baldi, P., Gramajo, H., & Tsai, S. C. (2006). Structure-based inhibitor design of AccD5, an essential acyl-CoA carboxylase carboxyltransferase domain of Mycobacterium tuberculosis. *Proceedings of the National Academy of Sciences of the United States of* America, 103(9), 3072–3077.

Liu J., Barry C. E. III, Besra G. S. and Nikaido H. (1996). Mycolic acid structure determines the fluidity of the mycobacterial cell wall. *Journal of Biological Chemistry* 271, 29545–29551.

Ma, Y., Stern, R. J., Scherman, M. S., Vissa, V. D., Yan, W., Jones, V. C., … McNeil, M. R. (2001). Drug targeting Mycobacterium tuberculosis cell wall synthesis: genetics of dTDP-rhamnose synthetic enzymes and development of a microtiter plate-based screen for inhibitors of conversion of dTDP-glucose to dTDP-rhamnose. *Antimicrobial agents and chemotherapy,* 45(5), 1407–1416.

The effect of pyrazinamide (aldinamide) on experimental tuberculosis in mice.

Malone L, Schurr A, Lindh H, Mckenzie D, Kiser JS, Williams H (1952) *Am Rev Tuberc*. 65(5):511-8.

Maria Rina, Charalambos Pozidis, Konstantinos Mavromatis, Maria Tzanodaskalaki, Michael Kokkinidis and Vassilis Bouriotis (2000) Alkaline phosphatase from the Antarctic strain TAB5 Properties and psychrophilic adaptations. *Eur. J. Biochem*. 267, 1230 ± 1238.

Michaelis, L., and Menten, M. L. (1913) Die Kinetik der Invertinwirkung. *Biochem*. Z. 49, 333–369

McCarthy, C. (1971). Utilization of palmitic acid by Mycobacterium avium. *Infect. Immun*. 4:199-204.

McIlleron H, Wash P, Burger A, Norman J, Folb PI & Smith P (2006) Determinants of rifampin, isoniazid, pyrazinamide, and ethambutol pharmacokinetics in a cohort of tuberculosis patients. *Antimicrob Agents Chemother* 50: 1170-1177.

McKinney JD, Honer zu Bentrup K, Munoz-Elias EJ, et al. (2000) Persistence of Mycobacterium tuberculosis in macrophages and mice requires the glyoxylate shunt enzyme isocitrate lyase. *Nature.* 406: 735-738.

Mdluli K, Kaneko T, Upton A (2014) Tuberculosis drug discovery and emerging targets. *Ann N Y Acad Sci*;1323:56-75.

Minnikin DE, Minnikin SM, Goodfellow M & Stanford JL (1982) The mycolic acids of Mycobacterium chelonei. *J Gen Microbiol* 128: 817-822.

Mudd S, Polevitzky K, Anderson TF & Chambers LA (1941) Bacterial Morphology as Shown by the Electron Microscope: II. The Bacterial Cell-wall in the Genus Bacillus. *J Bacteriol* 42: 251-264.

Nadav Elad, Szilvia Baron, Yoav Peleg, Shira Albeck, Jacob Grunwald, Gal Raviv, Zippora Shakked, Oren Zimhony & Ron Diskin (2018) Structure of Type-I Mycobacterium tuberculosis fatty acid synthase at 3.3 Å resolution. *Nature Communications*. Volume 9, Article number: 3886.

Navarathna DHMLP, Harris SD, Roberts DD, Nickerson KW (2010) Evolutionary aspects of urea utilization by fungi. *FEMS Yeast Res*. 10:209–213.

Neres, J., N.P. Labello, R.V. Somu, et al. (2008). Inhibition of siderophore biosynthesis in Mycobacterium tuber- culosis with nucleoside bisubstrate analogues: structure- activity relationships of the nucleobase domain of 5′-O- [N-(salicyl)sulfamoyl]adenosine. *J. Med. Chem.* 51: 5349– 5370.

Noens EE, Williams C, Anandhakrishnan M, Poulsen C, Ehebauer MT & Wilmanns M (2011) Improved mycobacterial protein production using a Mycobacterium smegmatis groEL1 C expression strain. *BMC Biotechnology* 11: 27.

Oh TJ, Daniel J, Kim H, Sirakova T & Kolattukudy PE (2006) Identification and Characterization of Rv3281 as a Novel Subunit of a Biotin-dependent Acyl-CoA Carboxylase in Mycobacterium tuberculosis H37Rv. *Journal of Biological Chemistry* 281: 3899-3908.

Olga Makarova, Emmanuel Kamberov & Ben Margolis (2018) Generation of Deletion and Point Mutations with One Primer in a Single Cloning Step. *Biotechniques*. Vol. 29, no. 5.

Oveimar Barbosa, Claudia Ortiz, Ángel Berenguer-Murcia, Rodrigo Torres, Rafael C. Rodrigue and Roberto Fernandez-Lafuente (2014) Glutaraldehyde in bio-catalysts design: a useful crosslinker and a versatile tool in enzyme immobilization. *RSC Advances* Issue 4, 1583-1600.

O'Garra A, Redford PS, McNab FW, Bloom CI, Wilkinson RJ, Berry MP (2013) The immune response in tuberculosis. *Annu Rev Immunol.* 31:475-527.

Paul TR & Beveridge TJ (1992) Reevaluation of envelope profiles and cytoplasmic ultrastructure of mycobacteria processed by conventional embedding and freeze-substitution protocols. *J Bacteriol* 174: 6508-6517.

Peroutka Iii RJ, Orcutt SJ, Strickler JE, Butt TR (2011) SUMO fusion technology for enhanced protein expression and purification in prokaryotes and eukaryotes. *Methods Mol Biol.* 705:15-30

Pitarque S, Larrouy-Maumus G, Payre B, Jackson M, Puzo G & Nigou J (2008) The immunomodulatory lipoglycans, lipoarabinomannan and lipomannan, are exposed at the mycobacterial cell surface. *Tuberculosis (Edinb*) 88: 560-565.

Portevin D, de Sousa-D'Auria C, Montrozier H, et al. (2005) The acyl-AMP ligase FadD32 and AccD4-containing acyl-CoA carboxylase are required for the synthesis of mycolic acids and essential for mycobacterial growth: identification of the carboxylation product and determination of the acyl-CoA carboxylase components. *J Biol Chem* 280: 8862-8874.

Qi Chen, Michal Vieth, David E. Timm, Christine Humblet, Dina Schneidman-Duhovny, Ilan E. Chemmama, Andrej Sali, Wei Zeng, Jirong Lu, Ling Liu (2017) Reconstruction of 3D structures of MET antibodies from electron microscopy 2D class averages. *PLoS One* 12 (4).

Rainer Kalscheuer, Ainhoa Palacios, Itxaso Anso, Javier Cifuente, Juan Anguita, William R. Jacobs Jr, Marcelo E. Guerin, Rafael Prados-Rosales (2019) The Mycobacterium tuberculosis capsule: a cell structure with key implications in pathogenesis. *Biochem J.* ; 476(14): 1995–2016.

Rendon, A., Tiberi, S., Scardigli, A., D'Ambrosio, L., Centis, R., Caminero, J. A., & Migliori, G. B. (2016). Classification of drugs to treat multidrug-resistant tuberculosis (MDR-TB): evidence and perspectives. *Journal of thoracic disease*, 8(10), 2666–2671.

Roberts. R. J (2005) How restriction enzymes became the workhorses of molecular biology. *Proceedings of the National Academy of Sciences*. 102 (17) 5905-5908.

Rodrigo Gay Ducati, Antonio Ruffino-Netto, Luiz Augusto Basso, Diógenes Santiago Santos (2006) The resumption of consumption – A review on tuberculosis. *Mem Inst Oswaldo Cruz, Rio de Janeiro,* Vol. 101(7): 697-714.

Rodriguez E & Gramajo H (1999) Genetic and biochemical characterization of the alpha and beta components of a propionyl-CoA carboxylase complex of Streptomyces coelicolor A3(2). *Microbiology* 145 (Pt 11): 3109-3119.

Rodriguez E, Banchio C, Diacovich L, Bibb MJ & Gramajo H (2001) Role of an Essential Acyl Coenzyme A Carboxylase in the Primary and Secondary Metabolism of Streptomyces coelicolor A3(2). *Applied and Environmental Microbiology* 67: 4166-4176.

Rodriguez, G.M. (2006). Control of iron metabolism in My- cobacterium tuberculosis*. Trends Microbiol.* 14: 320–327.

Rosano, G. L., & Ceccarelli, E. A. (2014). Recombinant protein expression in Escherichia coli: advances and challenges. *Frontiers in microbiology*, 5, 172.

Russell. D, Barry. C, Flynn. J (2010) Tuberculosis: What We Don't Know Can, and Does, Hurt Us. *Science.* 328(5980):852-6

Russell DG (2007) Who puts the tubercle in Tuberculosis? *Nat Rev Microbiol* 5: 39-47.

Russell DG, Cardona PJ, Kim MJ, Allain S & Altare F (2009) Foamy macrophages and the progression of the human tuberculosis granuloma. *Nat Immunol* 10: 943-948.

Salfullah Bullo, Mohd Zobir Hussein, Samer Hasan Hussein-Al-Ali (2012) Controlled-release approaches towards the chemotherapy of tuberculosis. *International Journal of Nanomedicine* 7:5451-63.

Sassetti CM, Boyd DH & Rubin EJ (2003) Genes required for mycobacterial growth defined by high density mutagenesis. *Mol Microbiol* 48: 77-84.

Sausen C.W., Rogers C.M., Bochman M.L. (2019) Thin-Layer Chromatography and Real-Time Coupled Assays to Measure ATP Hydrolysis. In: Balakrishnan L., Stewart J. (eds) DNA Repair. *Methods in Molecular Biology*, vol 1999.

Scarff, C. A., Fuller, M., Thompson, R. F., & Iadanza, M. G. (2018). Variations on Negative Stain Electron Microscopy Methods: Tools for Tackling Challenging Systems. *Journal of visualized experiments JoVE*, (132), 57199.

Schaaf HS, Thee S, van der Laan L, Hesseling AC, Garcia-Prats AJ (2016) Adverse effects of oral second-line antituberculosis drugs in children. *Expert Opin Drug Saf*. (10):1369-81.

Schlesinger LS (1993) Macrophage phagocytosis of virulent but not attenuated strains of Mycobacterium tuberculosis is mediated by mannose receptors in addition to complement receptors. *J Immunol* 150: 2920-2930.

Schatz Albert, Waksman S.A (1944) Effect of streptomycin and other antibiotic substances upon Mycobacterium tuberculosis and related organisms. *Proc., Soc. Exper. Biol.& Med*. 57: 244-248.

Shepherd RG, Baughn C, Cantrall ML, Goodstein B, Thomas JP, Wilkinson RG (1966) Structure-activity studies leading to ethambutol, a new type of antituberculous compound. *Ann N Y Acad Sci.* 135(2):686-710.

Showalter AM (2001) Arabinogalactan-proteins: structure, expression and function. *Cell Mol Life Sci.* ;58(10):1399-417.

Sibley LD, Hunter SW, Brennan PJ & Krahenbuhl JL (1988) Mycobacterial lipoarabinomannan inhibits gamma interferon-mediated activation of macrophages. *Infect Immun* 56: 1232-1236.

Simonian MH (2002) Spectrophotometric determination of protein concentration. *Protoc Cell Biol* Appendix 3:Appendix 3B.

Slusarewicz, P., Zhu, K., & Hedman, T. (2010). Kinetic characterization and comparison of various protein crosslinking reagents for matrix modification. Journal of materials science. *Materials in medicine*, 21(4), 1175–1181.

Smith S, Witkowski A & Joshi AK (2003) Structural and functional organization of the animal fatty acid synthase. *Prog Lipid Res* 42: 289-317.

Balaji Sundararaman, Kannan Palaniyandi, Arunkumar Venkatesan, Sujatha Narayanan (2014) Expression, purification and functional characterization of AmiA of acetamidase operon of Mycobacterium smegmatis. *Microbiological Research* 169 (11) 873–880.

Thongnuanchan, B., Ninjan, R., Kalkornsurapranee, E. et al (2018) Glutaraldehyde as Ambient Temperature Crosslinking Agent of Latex Films from Natural Rubber Grafted with Poly (diacetone acrylamide). *J Polym Environ*. 26, 3069–3085.

Tiengo, A., Barbarini, N., Troiani, S., Rusconi, L., & Magni, P. (2009). A Perl procedure for protein identification by Peptide Mass Fingerprinting. *BMC bioinformatics*. 10(Suppl 12): S11.

Ting-Wan Lin, Melrose M. Melgar, Daniel Kurth, S. Joshua Swamidass, John Purdon, Teresa Tseng, Gabriela Gago, Pierre Baldi, Hugo Gramajo, and Shiou-Chuan Tsai (2006) Structure-based inhibitor design of AccD5, an essential acyl-CoA carboxylase carboxyltransferase domain of Mycobacterium tuberculosis. *PNAS*. 103 (9) 3072-3077.

Tong L (2013) Structure and function of biotin-dependent carboxylases. *Cell Mol Life Sci.* 70(5):863-91.

Tong L (2017) Chapter Five - Striking Diversity in Holoenzyme Architecture and Extensive Conformational Variability in Biotin-Dependent Carboxylases. *Advances in Protein Chemistry and Structural Biology*. Volume 109. Pages 161-194.

Tran, T., Hsiao, Y., Jo, J. et al. (2015) Structure and function of a single-chain, multi-domain long-chain acyl-CoA carboxylase. Nature. 518, 120–124.

Trivedi OA, Arora P, Sridharan V, Tickoo R, Mohanty D & Gokhale RS (2004) Enzymic activation and transfer of fatty acids as acyl-adenylates in mycobacteria. *Nature* 428: 441-445.

Uhlmann, D. Oberschmidt, A. Spielvogel, K. Herms, M. Polte, J. Polte, A. Dumke (2013) Development of a versatile and continuously operating cell disruption device. *Procedia* CIRP 5 (2013) 119 – 123.

Ukai H, Ukai-Tadenuma M, Ogiu T, Tsuji H (2002) A new technique to prevent self-ligation of DNA. *J Biotechnol*. 97(3):233-42.

United Nations (2018) Political Declaration on TB 2018: United to End Tuberculosis: An Urgent Global Response to a Global Epidemic.

Van Crevel R, Ottenhoff TH & van der Meer JW (2002) Innate immunity to Mycobacterium tuberculosis. *Clin Microbiol Rev* 15: 294-309.

Van der WN, Hava D, Houben D, Fluitsma D, van ZM, Pierson J, Brenner M, Peters PJ (2007) M. tuberculosis and M. leprae translocate from the phagolysosome to the cytosol in myeloid cells. *Cell*. 129:1287–1298.

Vilcheze C, Morbidoni HR, Weisbrod TR, Iwamoto H, Kuo M, Sacchettini JC & Jacobs WR, Jr. (2000) Inactivation of the inhA-encoded fatty acid synthase II (FASII) enoyl-acyl carrier protein reductase induces accumulation of the FASI end products and cell lysis of Mycobacterium smegmatis. *J Bacteriol* 182: 4059-4067.

Vollmer, W., Blanot, D. and de Pedro, M. A. (2008). Peptidoglycan structure and architecture. *FEMS Microbiology Reviews* 32, 149–167.

Wang, Ignatius, and Thakkar (2014) Impact of Residual Impurities and Contaminants on Protein Stability. *Journal of Pharmaceutical Sciences*. Mini Review.

Wehrli W, Staehelin M (1971) Actions of the rifamycins. *Bacteriol Rev*. 35(3):290-309.

Wingfield P. T. (2015). Overview of the purification of recombinant proteins. Current protocols in protein science, 80, 6.1.1–6.1.35.

Wishart DS, Knox C, Guo AC, et al. (2006) DrugBank: a comprehensive resource for in silico drug discovery and exploration. *Nucleic Acids Res* 34: D668-672.

Wittig I, Beckhaus T, Wumaier Z, Karas M, Schägger H (2010) Mass estimation of native proteins by blue native electrophoresis: principles and practical hints. *Mol Cell Proteomics.* 9(10):2149–2161.

World Health Organization (WHO) (2019) Global Tuberculosis Report 2019.

Wright DH, Brown GH, Peterson ML & Rotschafer JC (2000) Application of fluoroquinolone pharmacodynamics. *J Antimicrob Chemother* 46: 669-683.

Wurth, C., Kessler, U., Vogt, J., Schulz, G. E., Folkers, G., & Scapozza, L. (2001). The effect of substrate binding on the conformation and structural stability of Herpes simplex virus type 1 thymidine kinase. *Protein science: a publication of the Protein Society*, 10(1), 63–73.

Zhang H, Boghigian BA, Pfeifer BA (2010) Investigating the role of native propionyl-CoA and methylmalonyl-CoA metabolism on heterologous polyketide production in Escherichia coli. *Biotechnol Bioeng*. 105:567–573.

Zhang, Y., Werling, U., & Edelmann, W. (2014). Seamless Ligation Cloning Extract (SLiCE) cloning method. *Methods in molecular biology* (Clifton, N.J.), 1116, 235–244.

Zheng J, Eric J. Rubin, Pablo Bifani, Vanessa Mathys, Vivian Lim, Melvin Au, Jichan Jang, Jiyoun Nam, Thomas Dick, John R. Walker, Kevin Pethe, Luis R. Camacho (2013) *J Biol Chem*. 288(32): 23447–23456.

Zhenzhan Chang, Jason Kuchar and Robert P. Hausinger (2004) Chemical Cross-linking and Mass Spectrometric Identification of Sites of Interaction for UreD, UreF, and Urease. *The Journal of Biological Chemistry.* 279, 15305-15313.

Zhong, J., Ye, Z., Lenz, S.W. et al (2017) Purification of nanogram-range immunoprecipitated DNA in ChIP-seq application. *BMC Genomics* 18, 985.

Zuber B, Chami M, Houssin C, Dubochet J, Griffiths G & Daffe M (2008) Direct visualization of the outer membrane of mycobacteria and corynebacteria in their native state. *J Bacteriol* 190: 5672-5680.

6. Appendix

Table 6.1: Bacterial expression vectors used in *E. coli* and *M. smegmatis* studies

Vector	Promoter	Resistance	Tag	Protease cleavage site	Source
pETM-11	T7/Lac	Kanamycin	N-ter His	TEV	G. Stier
pET SUMO-LIC	T7/Lac	Kanamycin	N-ter His N-ter SUMO	TEV	H. Meyerhofer
pMyNT	Acetamidase	Hygromycin	N-ter His	TEV	A. Geerlof
pMyC	Acetamidase	Kanamycin	N-ter His N-ter Strep	TEV	K. Beckham

Table 6.2: Bacterial strains used for this study

Strain	Description	Function	Source
E. coli DH5α	T1 phage-resistant	Cloning host (non-expression)	Life Technologies
E. coli BL21 (DE3)	Deficient in *Ion* and *ompT* proteases	Expression host	Novagen
E. coli BL21 star pRare	RNaseE *(rne131)* mutant. Addition of plasmids *argU, argW, argX, glyT, ileX, leuW, metT, proL, thrT, thrU and tyrU.*	Expression host with reduced mRNA degradation and additional rare tRNA codons	A. Geerlof
M. smegmatis groEL1ΔC	Deficient in C-terminal His-rich coding sequence	Efficient and specific purification of His-tagged proteins	Noens *et al.,* 2011

Table 6.3: Plasmid constructs used in this study

Construct ID	Protein	Gene	Vector	Resistance	Created by
M02	AccA3	Rv3285	pETM-11	Kanamycin	Simon, Oct '05
M03	AccA3	Rv3285	pMyNt	Hygromycin	Madhan, Feb '10
M06	AccD4	R3799c	pETM-11	Kanamycin	Simon, June '11
M07	AccD4	Rv3799c	pMyNt	Hygromycin	Simon, Jan '07
M08	AccD5	Rv3280	pETM-11-LIC	Kanamycin	Madhan, July '11
M09	AccD5-AccE5	Rv3280-Rv3281	pMyNt	Hygromycin	Madhan, Mar '11
M11	AccE5	Rv3281	pET SUMO-LIC	Kanamycin	Madhan, Mar '11
M38	AccD5-E5	Rv3280-Rv3281	pMyC	Kanamycin	Sonja, Jan '15

Bacterial growth media and electrophoresis components

Luria Broth (LB)

For LB medium, 20 g LB powder was dissolved in 1000 mL distilled water, sterilized by autoclaving and stored at room temperature. LB agar stocks were made using 37g LB agar powder dissolved in 1000 mL distilled water, sterilized by autoclaving and stored at room temperature. For pouring LB agar onto plates, LB agar stocks were melted using a microwave, cooled and poured with the appropriate antibiotic added. These were labelled and stored at 4 ^{o}C.

Antibiotics

1000X Kanamycin was made using a Kanamycin stock to make a 50 mg/mL solution in distilled water. 1000X Hygromycin was made using a Hygromycin stock to make a 50 mg/mL solution in distilled water. Solutions were filter-sterilized and stored in 1 mL aliquots at -20 ^{o}C.

Terrific Broth (TB)

TB was made using 47.6g TB powder and 4 mL glycerol dissolved in distilled water to a final volume of 1000 mL. These are sterilized by autoclaving and stored at room temperature.

Super optimal catabolite repression medium (SOC)

SOC is used for smaller volumes of bacteria, typically for use in plasmid isolation after colony PCR. This uses a combination of 2.5g Yeast Extract, 10g Tryptone, 1 mL 5M NaCl, 416 µL 3M KCl, 5 mL 1M $MgCl_2$, 5 mL 1M $MgSO_4$ and 495 mL distilled water. This was sterilized by autoclaving, cooled and 5 mL of 1M glucose was added prior to storage at 4 ^oC.

7H9 media

7H9 expression medium uses 4.7 g Middlebrook 7H9 medium powder (Merck) dissolved in 1000 ml distilled water and autoclaved. Immediately prior to use, 10 ml of 20% (w/v) glucose, 4 ml of 50% (v/v) glycerol and 2.5 ml of 20% (v/v) Tween 80 were added.

Acetamide solution

A 220X acetamide solution was made using 20g acetamide dissolved in 31 mL water. This was filter-sterilized and stored in a 50 mL falcon tube at 4 ^oC.

SDS-PAGE running buffer

A 10X buffer was made using 151.4g Tris base, 720g Glycine, 50g SDS and distilled water up to a 5 L solution.

Coomassie blue safe stain

0.8g Brilliant blue G-250 is added to 500 mL distilled water and dissolved with stirring overnight at 4 ^oC. 34mL of 32% (v/v) HCl is added and the volume was made to 1000 mL with distilled

water. The staining solution is stored at 4 ºC and protected from light. Increased concentrations (0.2-5%) of Brilliant Blue G-250 were made for running Native gels.

Native Gel PAGE de-staining solution

Native de-staining solutions were made with 20% (v/v) ethanol, 5% acetic acid (v/v) and 1% glycerol (w/v) in 500 mL distilled water. This was stored at 4 ºC.

Buffers for protein purification

All buffers were prepared using Mill-Q water from the Mill-Q Millipore system. Buffer pH values were measured using a S20-K SevenEasy pH meter from Mettler Toledo. Buffers were filtered (0.22 µm membrane filter) and de-gassed before use. See following pages for buffer compositions. Compositions are mostly taken from a previous study conducted at the same institute (Anandhakrishnan, 2013). The # symbol by a component indicates it should be added just prior to use.

Table 6.4: Optimised buffer compositions used for protein purification

Protein	Expression host	Expression conditions	Buffers for purification
AccA3, D4, D5, E5 (Construct M03, M07, M09, M38)	*M. smegmatis* *groEL1ΔC*	1X Acetamide 37°C 16 hours	**Lysis:** 50 mM Tris-HCl (pH 8.0), 300 mM NaCl, 0.2% (v/v) NP-40, 0.02% (v/v) 1-thioglycerol (TG) [#] **Binding:** 50 mM Tris-HCl (pH 8.0), 300 mM NaCl, 20 mM imidazole, 0.01% (v/v) 1-TG[#], 20% (v/v) glycerol **Wash:** 50 mM Tris-HCl (pH 8.0), 300 mM NaCl, 50 mM imidazole, 0.01% (v/v) 1-TG[#], 20% (v/v) glycerol **Elution:** 50 mM Tris-HCl (pH 8.0), 300 mM NaCl, 300 mM imidazole, 0.01% (v/v) 1-TG[#], 20% (v/v) glycerol **SEC:** 50 mM Tris-HCl (pH 8.0), 100 mM NaCl, 5% (v/v) glycerol, 1 mM TCEP[#]
AccA3 (Construct M02)	*E. coli* BL21 star (DE3) pRare2	0.3 mM IPTG 30°C 16 hours	**Lysis:** 50 mM HEPES (pH 7.5), 300 mM KCl, 0.2% (v/v) NP-40, 5% (v/v) glycerol, 1 mM β-ME[#] **Binding:** 50 mM HEPES (pH 7.5), 300 mM KCl, 20 mM imidazole, 5% (v/v) glycerol, 1 mM β-ME[#] **Wash:** 50 mM HEPES (pH 7.5), 300 mM KCl, 50/75 mM imidazole, 5% (v/v) glycerol, 1 mM β-ME[#] **Elution:** 50 mM HEPES (pH 7.5), 300 mM KCl, 300 mM imidazole, 5% (v/v) glycerol, 1 mM β-ME[#] **SEC:** 50 mM HEPES (pH 7.5), 300 mM KCl, 5% (v/v) glycerol, 1 mM TCEP[#]

Protein	Expression host	Expression conditions	Buffers for purification
AccD4, E5 (Construct M06, M11)	*E. coli* BL21 (DE3)	0.5 mM IPTG 21°C 16 hours	**Lysis:** 50 mM Tris-HCl (pH 8.0), 150 mM NaCl, 0.2% (v/v) NP-40 **Binding:** 50 mM Tris-HCl (pH 8.0), 150 mM NaCl, 20 mM imidazole, 10% glycerol **Wash:** 50 mM Tris-HCl (pH 8.0), 150 mM NaCl, 50/75 mM imidazole, 10% glycerol **Elution:** 50 mM Tris-HCl (pH 8.0), 150 mM NaCl, 250 mM imidazole, 10% glycerol **Dialysis prior to methylation:** 50 mM HEPES (pH 7.5), 150 mM NaCl **SEC:** 50 mM Tris-HCl (pH 8.0), 150 mM NaCl, 5% glycerol, 2 mM DTT [#]
AccD5 (Construct M08)	*E. coli* BL21 star (DE3) pRare2	0.25 mM IPTG 18°C 16 hours	**Lysis:** 50 mM Tris-HCl (pH 8.0), 100 mM NaCl, 0.2% (v/v) NP-40, 0.02% (v/v) 1-TG[#] **Binding:** 50 mM Tris-HCl (pH 8.0), 150 mM NaCl, 20 mM imidazole, 0.01% (v/v) 1-TG[#] **Wash:** 50 mM Tris-HCl (pH 8.0), 200 mM NaCl, 50 mM imidazole, 0.01% (v/v) 1-TG[#] **Elution:** 50 mM Tris-HCl (pH 8.0), 200 mM NaCl, 300 mM imidazole, 0.01% (v/v) 1-TG[#] **SEC:** 50 mM Tris-HCl (pH 8.0), 200 mM NaCl, 2% (v/v) glycerol, 2 mM DTT[#]

Table 6.5: Kinetic Assay Mixture to measure ACCase activity

	Stock concentration (M)		In well						Master Mix (triplicster Mix (1 curve)					Final concentra
K_2HPO_4 pH 7.6	1		10	10	10	10	10	10		**200**	**70**			0.1
$MgCl_2$	1		0.5	0.5	0.5	0.5	0.5	0.5		**10**	**3.5**			0.005
$NaHCO_3$	1		4.8	4.8	4.8	4.8	4.8	4.8		**96**	**33.6**			0.048
ATP	0.1		3	3	3	3	3	3		**60**	**21**			0.003
β-NADH	0.1		0.2	0.2	0.2	0.2	0.2	0.2		**4**	**1.4**			0.0002
bovine serum albumin (BSA)	10 mg/ml		3	3	3	3	3	3		**60**	**21**			0.3 mg/ml
phosphoenolpyruvate (PEP)	0.1		0.5	0.5	0.5	0.5	0.5	0.5		**10**	**3.5**			0.0005
lactate dehydrogenase /pyruvate kinase	1000U/700U		1	1	1	1	1	1		**20**	**7**			10U/7U
sub-total			**23**	**23**	**23**	**23**	**23**	**23**		460	161			-
acyl-CoA	0.05 M		**0**	**1.25**	**2.5**	**5**	**10**	**20**						0-0.01
H2O	-		**27**	**25.75**	**24.5**	**22**	**17**	**7**						-
ACCase	0.75 mg/ml		**50**	**50**	**50**	**50**	**50**	**50**						0.35 mg/ml
Total	-		**100**	**100**	**100**	**100**	**100**	**100**						
			1	2	3	4	5	6	7	8	9	10	11	12
	96-well plate	A	0	7.8	13.3	18.1	20.2	21.2						
	UV-Star	B	0	9.3	11.8	16.9	19.2	19.9						
		C	0	8.5	14.9	16.7	18.3	22.2						
		D												
		E												
		F												
		G												
		H												
		Average	0.00	8.53	13.33	17.23	19.23	21.10						
		SE	0	0.43	0.90	0.44	0.55	0.67						

Acknowledgements

Ehmke Pohl (Durham University supervisor)

Matthias Wilmanns (EMBL Hamburg group leader)

Edu Mullapudi (EMBL Hamburg supervisor)

Kate Beckham (Staff Scientist)

And to the remaining EMBL Wilmanns group members.